

ANALYSIS AND DESIGN OF PASSIVE MICROWAVE AND OPTICAL
DEVICES USING THE MULTIMODE INTERFERENCE TECHNIQUE

A THESIS SUBMITTED TO
THE GRADUATE SCHOOL OF NATURAL AND APPLIED SCIENCES
OF
MIDDLE EAST TECHNICAL UNIVERSITY

BY

AHMET SERTAÇ SUNAY

IN PARTIAL FULFILLMENT OF THE REQUIREMENTS
FOR
THE DEGREE OF MASTER OF SCIENCE
IN
ELECTRICAL AND ELECTRONICS ENGINEERING

JUNE 2005

Approval of the Graduate School of Natural and Applied Sciences.

Prof. Dr. Canan Özgen
Director

I certify that this thesis satisfies all the requirements as a thesis for the degree of Master of Science.

Prof. Dr. İsmet Erkmen
Head of Department

This is to certify that we have read this thesis and that in our opinion it is fully adequate, in scope and quality, as a thesis for the degree of Master of Science.

Prof. Dr. Tuncay Birand
Supervisor

Examining Committee Members

Prof. Dr. Canan Toker (METU, EE) _____

Prof. Dr. Tuncay Birand (METU, EE) _____

Prof. Dr. Altuncan Hızal (METU, EE) _____

Prof. Dr. Gönül Turhan Sayan (METU, EE) _____

Dr. Bülent Yılmaz (Baskent Univ., BME) _____

I hereby declare that all information in this document has been obtained and presented in accordance with academic rules and ethical conduct. I also declare that, as required by these rules and conduct, I have fully cited and referenced all material and results that are not original to this work.

Ahmet Sertay Sunay

ABSTRACT

ANALYSIS AND DESIGN OF PASSIVE MICROWAVE AND OPTICAL DEVICES USING THE MULTIMODE INTERFERENCE TECHNIQUE

Sunay, Ahmet Sertaç

M.S., Department of Electrical and Electronics Engineering

Supervisor: Prof. Dr. Tuncay Birand

July 2005, 101 pages

The Multi Mode Interference (MMI) mechanism is a powerful tool used in the analysis and design of a certain class of optical, microwave and millimeter wave devices.

The principles of the MMI method and the self-imaging principle is described. Using this method, $N \times M$ MMI couplers, MMI splitter/combiners are analyzed.

Computer simulations for illustrating the "Multimode Interference Mechanism" and "Multimode Interference Couplers" are carried out.

The MMI approach is used to analyze overmoded 'rectangular metallic' and 'dielectric slab' type of waveguides and devices.

The application of the MMI technique is investigated experimentally by using a metallic waveguide structure operating in the X-band. The construction of the related structure and the related experimental work are reported.

Keywords: Multimode Interference, Couplers, Dielectric slab Waveguides, Rectangular Waveguides.

ÖZ

PASİF MİKRODALGA VE OPTİK ARAÇLARIN ÇOKLU MODLARIN GİRİŞİMİ TEKNIĞİ KULLANILARAK ANALİZ VE TASARIMLARI

Sunay, Ahmet Sertaç

Yüksek Lisans, Elektrik – Elektronik Mühendisliği Bölümü

Tez Yöneticisi: Prof. Dr. Tuncay Birand

Temmuz 2005, 101 sayfa

Çoklu Modların Girişimi tekniği (MMI) bazı optik, mili metrik dalga ve mikro dalga aygıtlarının analiz ve tasarımlarında kullanılan güçlü bir araçtır.

MMI yönteminin temel prensipleri ve kendini görüntüleme prensibi tanıtıldı. Bu yöntem kullanılarak, $N \times N$ MMI çoklayıcıları, MMI ayırıcı/birleştiricileri incelendi.

Çoklu Modların Girişimi ve Çoklu Modların Girişim Birleştiricilerini örneklemek amacıyla bilgisayar simülasyonları gerçekleştirildi.

Çok modlu 'dikdörtgen metalik' ve 'dielektrik kat' dalga kılavuzları ve araçlarının analizi için MMI yaklaşımı kullanıldı.

MMI tekniđinin uygulanmasının deneysel olarak arařtırılması amacıyla X-bantta alıřan bir metalik dalga kılavuzu kullanıldı. İlgili yapının kurulumu ve ilgili deneysel alıřma rapor edildi.

Anahtar Kelimeler: oklu Modların Giriřimi, Birleřtiriciler, Dielektrik kat dalgakılavuzları, Dikdörtgen dalga kılavuzları.

To my Parents

ACKNOWLEDGMENTS

The author wishes to express his deepest gratitude to his supervisor Prof. Dr. Tuncay Birand for his guidance, advice, criticism and encouragement throughout the research.

The author wishes to thank Prof. Dr. Altunkal Hızal to his valuable advice and contributions during the experimental phase.

TABLE OF CONTENTS

PLAGIARISM	iii
ABSTRACT	iv
ÖZ	vi
DEDICATION	viii
ACKNOWLEDGMENTS	ix
TABLE OF CONTENTS	x
LIST OF FIGURES	xii
LIST OF SYMBOLS	xiv

CHAPTER

1 INTRODUCTION	1
2 THE MULTIMODE INTERFERENCE METHOD	4
2.1 The Multimode Interference Method and its Application to Optical Devices	4
2.2 The Self – Imaging Principle	5
2.3 Analysis of Optical Devices	10
2.3.1 2×2 MMI Couplers	10
2.3.2 1×2 MMI Power Splitters	13
3 ANALYSIS OF RECTANGULAR WAVEGUIDES USING THE MMI METHOD	16
3.1 Introduction	16
3.2 Formulation	17
3.3 Simulation Results	19
4 ANALYSIS OF MICROWAVE AND MILLIMETER WAVE DIELECTRIC WAVEGUIDE SYSTEMS	26
4.1 Introduction	26
4.2 Formulation	26
4.3 Simulation Results	28

5	EXPERIMENTAL INVESTIGATIONS: MULTIMODED RECTANGULAR WAVEGUIDE SECTION	36
5.1	Construction of the Multimoded H-Plane Rectangular Structure	36
5.2	Experiments	37
5.3	Discussions	45
6	CONCLUSIONS	46
	REFERENCES	47
	APPENDICES	
A	ANALYSIS OF OPTICAL SLAB WAVEGUIDES	51
A.1	Theoretical Background	51
A.2	Wave Optics: Solution of Wave Equation.	52
A.2.1	Introduction	52
A.2.2	Wave Equation	53
A.3	Guided Modes of the Slab Waveguide	57
A.3.1	TE Modes	58
A.3.1.1	Even Guided TE Modes	59
A.3.1.2	Odd Guided TE Modes	60
A.3.1.3	Eigenvalues of TE Modes	61
A.3.2	TM Modes	62
A.3.2.1	Even Guided TM Modes	62
A.3.2.2	Odd Guided TM Modes	63
A.4	Solution of Eigenvalue Equations	64
A.5	Goos – Haenchen Shift	67
B	ANALYSIS OF RECTANGULAR WAVEGUIDES	69
B.1	TE Waves	71
B.2	TM Waves	74
C	ANALYSIS OF DIELECTRIC IMAGE LINES	77
D	MATLAB CODES	80

LIST OF FIGURES

2.1	Top View of a MMI device	5
2.2	Multimode Interference Coupler	10
2.3	Input-output graphs for 2×2 Silica based MMI coupler . . .	11
2.4	Phase characteristics of silica based MMI coupl	12
2.5	Input-output graphs for 2×2 InP-based MMI coupler . . .	13
2.6	Multimode Interference Splitter	14
2.7	Input-output graphs for 1×2 Silica based MMI coupler . . .	15
3.1	Schematic Diagram of $N \times M$ MMI Device	17
3.2	Dispersion characteristics of the rectangular waveguide . . .	20
3.3	Input – output graphic of MMI section at propagation distance $L = 21.8$ cm	21
3.4	Input – output graphic of MMI section at propagation distance $L = 11$ cm	22
3.5	Phase characteristics of the MMI structure at propagation distance $L = 11$ cm	23
3.6	Input – output graphic of MMI section at propagation distance $L = 7.8$ cm	24
3.7	3-D simulation of 1×2 MMI coupler	25
3.8	First seven E_y propagating modes	25
4.1	Cross section of dielectric image guide	27
4.2	3-Dimensional representation of an image guide using MMI approach	28
4.3	A number of modes in the dielectric image line ($2a = 2.2$ cm. $b = 0.58$ cm. $\epsilon_r = 4$)	29
4.4	Simulation result for propagation distance $L = 13.7$ cm	30

4.5	Simulation result for propagation distance $L = 10.1$ cm . . .	30
4.6	Simulation result for propagation distance $L = 4.9$ cm . . .	31
4.7	Simulation result for propagation distance $L = 18.1$ cm . . .	31
4.8	Phase characteristics of the input and two-output ports for the dielectric MMI structure	32
4.9	3-D plotting of the 1×2 MMI coupler	34
4.10	First six E_y propagating modes	34
5.1	Experimental setup	39
5.2	Plots of the $ E_y $ versus distance over the aperture plane with frequency 9 GHz	40
5.3	Plots of the $ E_y $ versus distance over the aperture plane with frequency 10 GHz	41
5.4	Plots of the $ E_y $ versus distance over the aperture plane with frequency 11 GHz	42
5.5	Plots of the $ E_y $ versus distance over the aperture plane with frequency 12 GHz	43
5.6	Plots of the $ E_y $ versus distance over the aperture plane with frequency 14 GHz	44
A.1	Cross Sectional view of a slab Waveguide	57
A.2	Even TE and Odd TE modes of slab waveguide	59
A.3	The Goos-Hanchen shift D of a beam of reflected light	68
A.4	Goos-Hanchen shifts on the waveguide	69
B-1	Cross section of rectangular waveguide	70
C.1	Dielectric image guide	77
C.2	Cross section of image guide	77
C.3	Field Distribution of the fundamental mode E_{11}^y	78

LIST OF SYMBOLS

MMI	:	Multimode Interference
WG	:	Waveguide
GHz	:	GigaHertz
MMPS	:	Multimode Power Splitter
TMI	:	Two-Mode Interference
InP	:	Indium-Phosphorus
Al_2O_3	:	Aluminum Oxide
SiO_2	:	Silicon oxide
MPA	:	Guided – Mode Propagation Analyses.
SI	:	Spectral Index Method
EIM	:	Effective Index Method

CHAPTER 1

INTRODUCTION

The Multi Mode Interference (MMI) method is a powerful tool used in the analysis and design of a certain class of optical devices. The MMI method may also be applied to simplify the analysis of some microwave and millimeter waveguide devices.

The MMI method is based on the self-imaging mechanism, which says that an input field profile is reproduced in single or multiple images at certain periodic intervals along the propagation direction of the guide.

Talbot described self-imaging of periodic objects more than 150 years ago [1]. Marcuse explained that graded index waveguides could also produce periodic images at certain propagation distances [2].

Bryngdahl and Ulrich have worked on self-imaging in uniform index slab waveguides [3],[4],[5]. Physical model of structure is naturally three-dimensional. 3 - D analysis of MMI couplers were described by Vazques [6].

Guided-mode propagation analysis (MPA) can be to understand the self-imaging phenomena in multimoded waveguides.

The fundamental principle of the MPA approach is simple; it decomposes an input field into all guided mode fields, propagates each of these modes independently, and calculates the output field by recombining the propagated mode fields.

Making use of the 'Spectral Index Method' or the effective index method (EIM), the problem can be cast into a two dimensional form [7],[8].

Soldano has described integrated optical device designs based on the MMI method [9],[10].

Knox and Toullos have developed the basics of the effective dielectric constant method (EDM) to analyze wave propagation in dielectric slab waveguides [11]. As shown by Ulrich The EDM method can be used to derive the eigenvalue equations and the equation for the axial propagation constant [12].

In recent years, there has been a growing tendency towards the application of multimode interference (MMI) effects in integrated optics. Application of the MMI method and the self-imaging principle used in analyzing optical devices are explained in Chapter 2. $N \times M$ MMI couplers, MMI splitter/combiners are analyzed and the results of computer simulations illustrating the Multimode Interference Mechanism and the Multimode Interference Couplers are presented in that chapter.

Metallic waveguides (WGs) and dielectric slab WGs are devices, which are widely used in telecommunication systems. The MMI approach can also be used to analyze such waveguides and related devices. In Chapter 3, the application of the MMI method together with the self-imaging principle to rectangular waveguides is presented. Mathematical model is given and computer simulation results are provided.

Dielectric slab waveguides operating at millimeter and microwave frequencies are analyzed in Chapter 4, using the MMI approach.

To investigate the application of the MMI technique experimentally, a metallic waveguide structure operating in the X band was designed. The construction of the related structure and the experimental work carried out are reported in Chapter 5. Both measurement and computer results are reported and compared.

CHAPTER 2

THE MULTIMODE INTERFERENCE METHOD

2.1 The Multimode Interference Method and its Application to the Analysis of Optical Devices

In this chapter, the MMI method is introduced and the underlying principles of this method are discussed. Then the principle of operation of the Multimode Interference (MMI) devices at optical frequencies is discussed.

The MMI method can be used to analyze and to design the optical, microwave and millimeter wave systems. The multimode interference method was first used in the analysis of optical devices. Therefore we first study the applications of this method by considering optical devices.

The mechanism of the MMI method is based on the principle of self-imaging, which is described in Section 2.2. To this end, a simple mathematical formula is derived.

Considering optical waveguides, one encounters the problem of the displacement of direction of reflected beam, which is not expected to be in accordance with the simple geometrical theory.

Goos–Haenchen shift is used to overcome this interesting phenomenon. It is described in Appendix A.5.

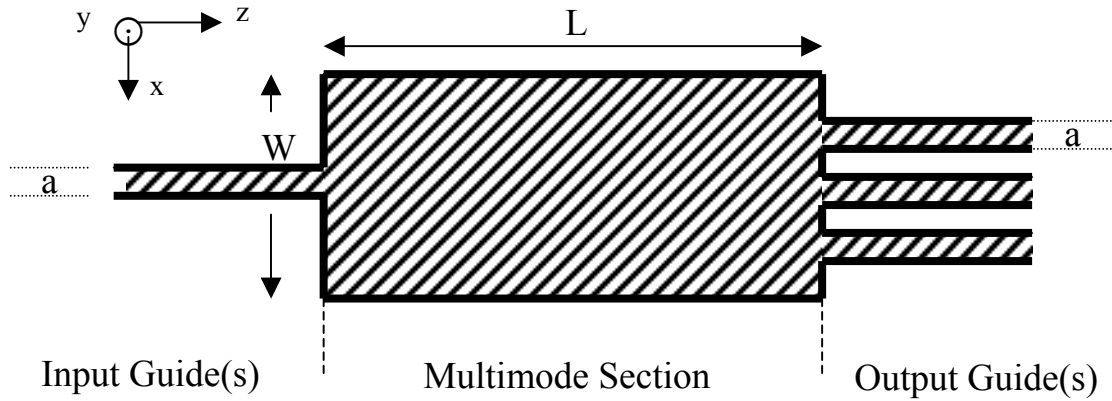


Figure 2.1 Top view of a MMI device.

2.2 The Self-Imaging Principle

The self-imaging principle may be stated as:

“Self imaging is a property of multimode waveguides by which an input field profile is reproduced in single or multiple images at periodic intervals along the increasing direction of the guide”

We use optical frequencies in this part of the report. Physical model is given in Figure 2.1.

Analysis is based on the mechanism, which decomposes an input field into all guided mode fields, then propagates each of these modes independently, and calculates the output field by recombining the propagated mode fields. The mechanism is called Multimode Interference.

An input field (signal) at $z=0$ can be decomposed into modal field distributions $\psi_v(y)$ of all modes as follows;

$$\Psi(y, 0) = \sum_{v=0}^{M-1} c_v \psi_v(y) \quad (2.1)$$

where M is the number of guided (propagation) modes, and field excitation coefficients c_v are given by

$$c_v = \frac{\int \Psi(y, 0) \psi_v^*(y) dy}{\int |\psi_v(y)|^2 dy} \quad (2.2)$$

$\psi_v(y)$ is the lateral field profile of the v^{th} mode.

Thus, equation (2.1) can be thought as Fourier series expansion. Each mode has excitation coefficient c_v , and these excitation coefficients are the Fourier series coefficients of each mode. Fundamental mode always has the higher excitation coefficient (and also propagation constant) and as the number of the modes increases, the value of excitation coefficient decreases just like Fourier series coefficients.

Because of this, choosing $\psi_v(y)$ as exponential function is very logical and it conforms to the idea of self-imaging method.

The field profile $\Psi(y, z)$ at the propagation distance z is approximately expressed by the superposition of M guided modes and is represented as follows;

$$\Psi(y, z) = \sum_{v=0}^{M-1} c_v \psi_v(y) e^{[j(\omega t - \beta_v z)]} \quad (2.3)$$

where β_v is the propagation constant of v^{th} mode.

The dispersion equation for a rib waveguide is

$$\kappa^2 + \beta_v^2 = k_0^2 n_1^2 \quad (2.4)$$

n_1 is the ridge (effective) refractive index of the waveguide. With

$$k_0 = \frac{2\pi}{\lambda} \quad (2.5)$$

Obtaining the lateral wave number for a slab waveguide is given in appendix A. From equation (A-90)

$$\kappa = \frac{(v+1)\pi}{W_M} \quad (2.6)$$

Using the Goos-Haenchen shift for W_M

$$\kappa = \frac{(v+1)\pi}{W_{ev}} \quad (2.7)$$

The effective width W_{ev} is given in appendix A. From equations (A.91) and (A.92)

For TE Modes
$$W_{ev} - W_M = \frac{\lambda_0}{\pi (n_1^2 \sin^2 \theta_1 - n_2^2)^{1/2}} \quad (2.8)$$

For TM Modes
$$W_{ev} - W_M = \frac{[\lambda_0 n_2^2 / n_1^2]}{\pi (n_1^2 \sin^2 \theta_1 - n_2^2)^{1/2}} \quad (2.9)$$

Dispersion equation for the structure is

$$\beta_v = \sqrt{k_0^2 n_1^2 - \kappa^2} \quad (2.10)$$

By using the binomial expansion with $\kappa^2 \ll k_0^2 n_1^2$; the propagation constants β_v can be deduced from equations (2.4), (2.5) and (2.7). For any power of n , the binomial $(a+x)$ can be expanded as follows

$$(a+x)^n = \sum_{k=0}^n \frac{n!}{(n-k)!k!} a^{n-k} x^k \quad (2.11)$$

Binomial expansion for $(k_0^2 n_1^2 - \kappa^2)^{1/2}$ is

$$\begin{aligned} (k_0^2 n_1^2 - \kappa^2)^{1/2} &= (k_0^2 n_1^2)^{1/2} - \frac{1}{2} (k_0^2 n_1^2)^{-1/2} \kappa^2 \Rightarrow \\ &= k_0 n_1 - \frac{1}{2k_0 n_1} \kappa^2 \\ &= k_0 n_1 - \frac{(v+1)^2 \pi \lambda}{4n_1 W_{ev}^2} \end{aligned} \quad (2.12)$$

The time dependence in formulation (2.3) can be dropped.

$$\Psi(y, z) = e^{j\beta_0 z} \sum_{v=0}^{M-1} c_v \Psi_v(y) e^{-j(\beta_0 - \beta_v)z} \quad (2.13)$$

β_0 could be found by using equation (2.10)

$$\beta_0 = k_0 n_1 - \frac{(0+1)^2 \pi \lambda}{4n_1 W_{ev}^2} = k_0 n_1 - \frac{\pi \lambda}{4n_1 W_{ev}^2} \quad (2.14)$$

The exponential part of equation (2.13) depends on $\beta_0 - \beta_v$

$$\begin{aligned}\beta_0 - \beta_v &= \left[k_0 n_1 - \frac{\pi \lambda}{4 n_1 W_{ev}^2} \right] - \left[k_0 n_1 - \frac{(\nu+1)^2 \pi \lambda}{4 n_1 W_{ev}^2} \right] \\ &= \frac{\pi \lambda (-1 + \nu^2 + 2\nu + 1)}{4 n_1 W_{ev}^2} \\ \beta_0 - \beta_v &= \frac{\pi \lambda \nu (\nu + 2)}{4 n_1 W_{ev}^2}\end{aligned}\quad (2.15)$$

Beat length of two-lowest order modes defined as

$$L_\pi = \frac{\pi}{\beta_0 - \beta_1} \quad (2.16)$$

β_1 could be found by using equation (2.10)

$$\beta_1 = k_0 n_1 - \frac{(1+1)^2 \pi \lambda}{4 n_1 W_{ev}^2} = k_0 n_1 - \frac{4\pi \lambda}{4 n_1 W_{ev}^2} \quad (2.17)$$

Inserting β_0 and β_1 into beat length equation, beat length can be rewritten as

$$\begin{aligned}L_\pi &= \frac{\pi}{k_0 n_1 - \frac{\pi \lambda}{4 n_1 W_{ev}^2} - k_0 n_1 + \frac{4\pi \lambda}{4 n_1 W_{ev}^2}} \\ L_\pi &= \frac{4 n_1 W_{ev}^2}{3\lambda}\end{aligned}\quad (2.17)$$

A useful expression for the field at distance $z=L$ is then found by substituting equation (2.17) into equation (2.13)

$$\Psi(y, L) = \sum_{v=0}^{m-1} c_v \psi_v(y) \exp \left[j \frac{v(v+2)\pi}{2L_\pi} L \right] \quad (2.18)$$

2.3 Analysis of Optical Devices

Numerical simulations of basic passive multimode interference couplers and splitter/combiners are presented in this section. Soldano has demonstrated the fabrication of a series of 2×2 MMI coupler and 1×2 the MMI splitters [13],[14].

2.3.1 2×2 MMI Couplers

Optical couplers are key components used in photonic integrated circuits for signal routing and signal processing. Two-Mode Interference (TMI) couplers consist of a two-moded central waveguide connected to two pairs of single-moded access waveguide, as shown in Figure 2.2.

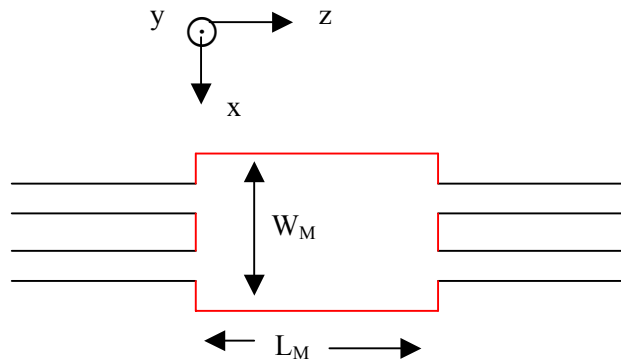


Figure 2.2 Multimode Interference Coupler.

Simulation studies were carried out for silica based aluminum oxide waveguide and In-P based waveguide structures. Silica based waveguide was composed of a rib-shaped Al_2O_3 guiding film sandwiched between two SiO_2 cladding layers. The refractive indices are $n(Al_2O_3)=1.679$ and $n(SiO_2)=1.444$.

Dimensions of the multimode section are $L_M=250\mu m$. length and $W_M=14\mu m$. width. Operation wavelength is given $\lambda=1520nm$. The gap between two input waveguides is nearly $4\mu m$.

Numerical simulation for 2×2 MMI silica based waveguide is illustrated in figure 2.3. In following input-output graphics, the horizontal axis is the x axis (micrometer) and the vertical axis presents the y axis (micrometer) as shown in Figure 2.2.

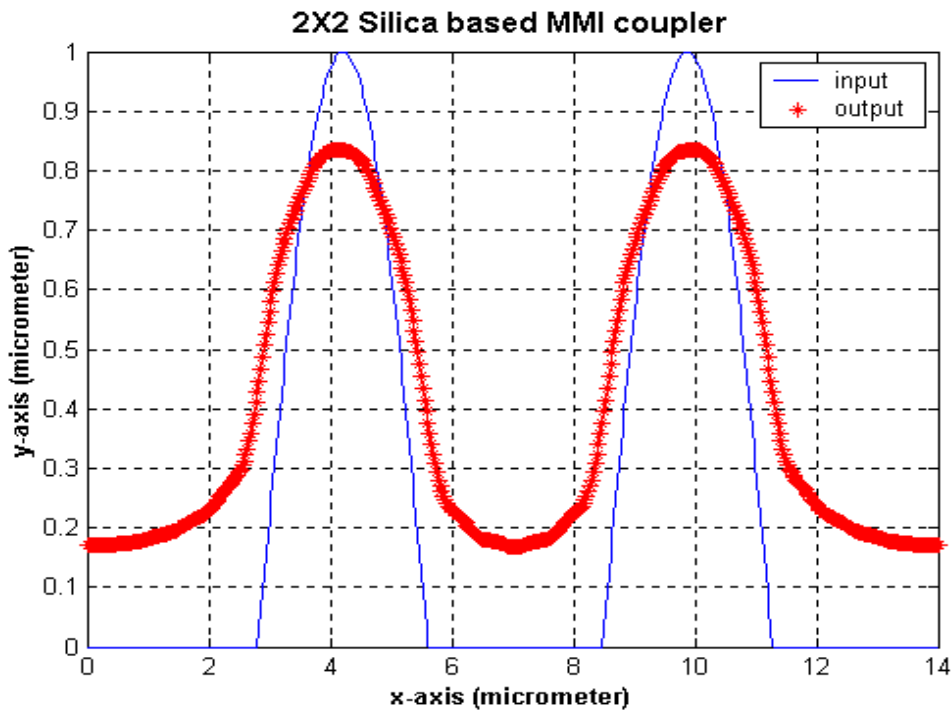


Figure 2.3 Input-output characteristics of silica based MMI coupler.

In figure 2.4, phase characteristics of the input and two-output ports for the 2×2 MMI coupler are shown.

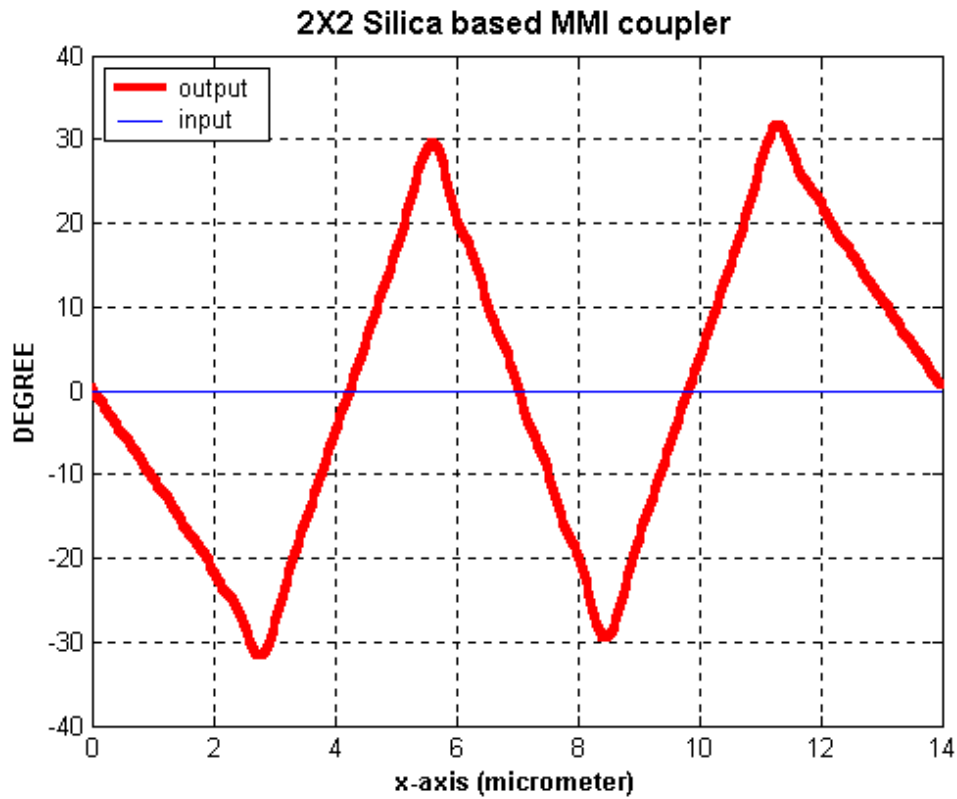


Figure 2.4 Phase characteristics of silica based MMI couple.

We can say that, there are no phase differences or phase shifts between two output ports of the MMI structure.

InP-based waveguide is composed of an InGaAsP (band-edge absorption wavelength $\lambda_g = 1.3\mu m$.) guiding layer sandwiched between two InP layers. The refractive indices are $n(\text{InGaAsP}) = 3.35$ and $n(\text{InP}) = 3.17$. Dimensions of the multimode section are $L_M = 420\mu m$ length and $W_M = 16\mu m$ width. Operation wavelength is given $\lambda = 1.52\mu m$. The gap between two input waveguides is nearly $6\mu m$. Result of our simulation for the 2×2 InP-based MMI coupler is illustrated in figure 2.5.

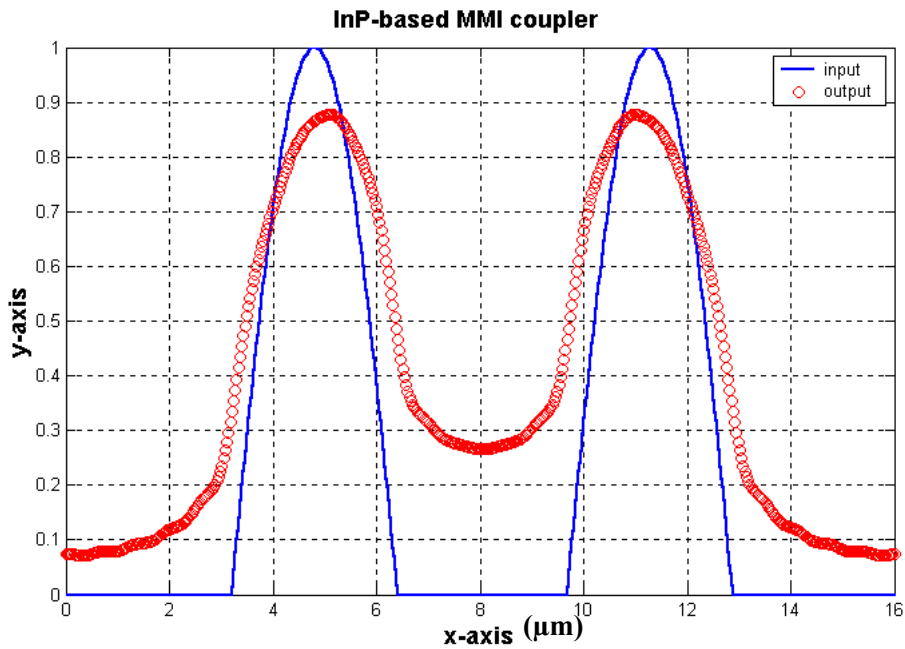


Figure 2.5 Input-output characteristics of InP-based MMI coupler.

2.3.2 1×2 MMI Power Splitters

The Multimode Power Splitter (MMPS) is based on the principle of symmetrical modal interference in a multimode section. A single mode input waveguide is positioned symmetrically around a multimode

waveguide. The length of the multimode interference sections is determined by the beating between the fundamental and second order symmetric MMI modes [15],[16]. The structure for MMI splitter is shown in figure 2.6.

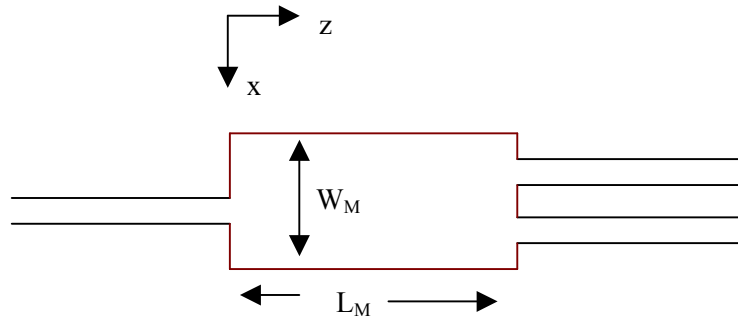


Figure 2.6 Multimode Interference Splitter.

In this section, simulation results for the silica based 1×2 MMI Power splitter is provided. The operation wavelength is given $\lambda = 1520nm$. Dimensions of the multimode section are $L_M = 21\mu m$. length and $W_M = 5.2\mu m$. width. The gap between two-output waveguides is nearly $1.7\mu m$. We simulated the 1×2 InP-based MMPS and illustrated the result in figure 2.7. Simulations reveal that equi-phase; balanced power partition from one single-moded input guide into two single-moded output guides is obtained.

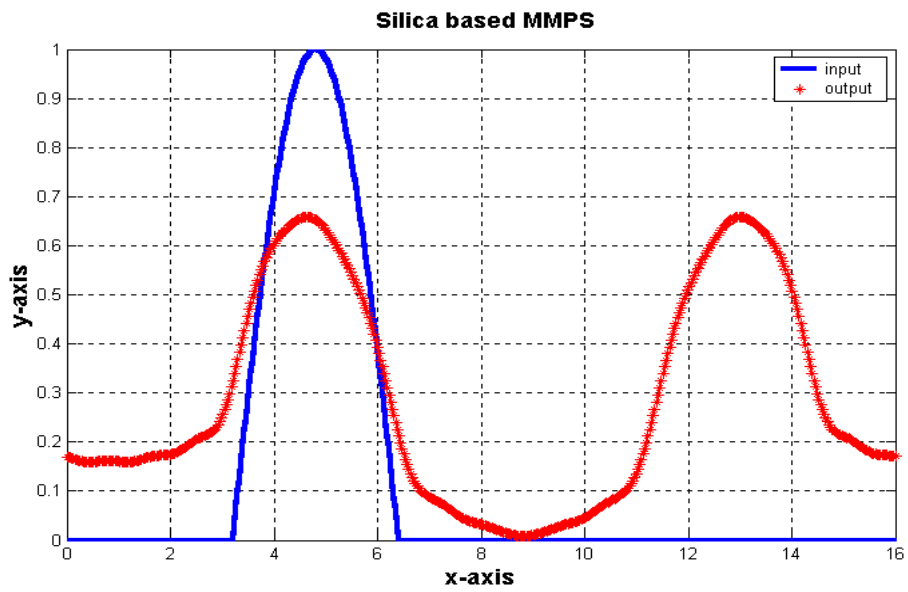


Figure 2.7 Input-output characteristics of 1×2 Silica based MMI coupler.

It is concluded that the MMI method is a powerful and useful tool to analyze and design optical devices such as power splitter/combiners and 3-dB couplers.

CHAPTER 3

ANALYSIS OF RECTANGULAR WAVEGUIDES USING THE MMI METHOD

3.1 Introduction

Rectangular waveguides are used in many practical communication systems. The objective of this chapter is to use of the Multimode Interference Method (MMI) in analyzing and designing certain rectangular passive WG devices.

The structure under investigation is shown in figure 3.1. Input section consists of a rectangular waveguide and in the MMI section, the input waveform is decomposed into modal fields and it is expected to reproduce itself at a distance $z = L$. If desired, the final output sections may consist of horn antennas. Thus one can realize the design of an antenna array feed network using the MMI method.

Conventional analyses of rectangular waveguides can be found in Colin and Balanis and elsewhere [17],[18].

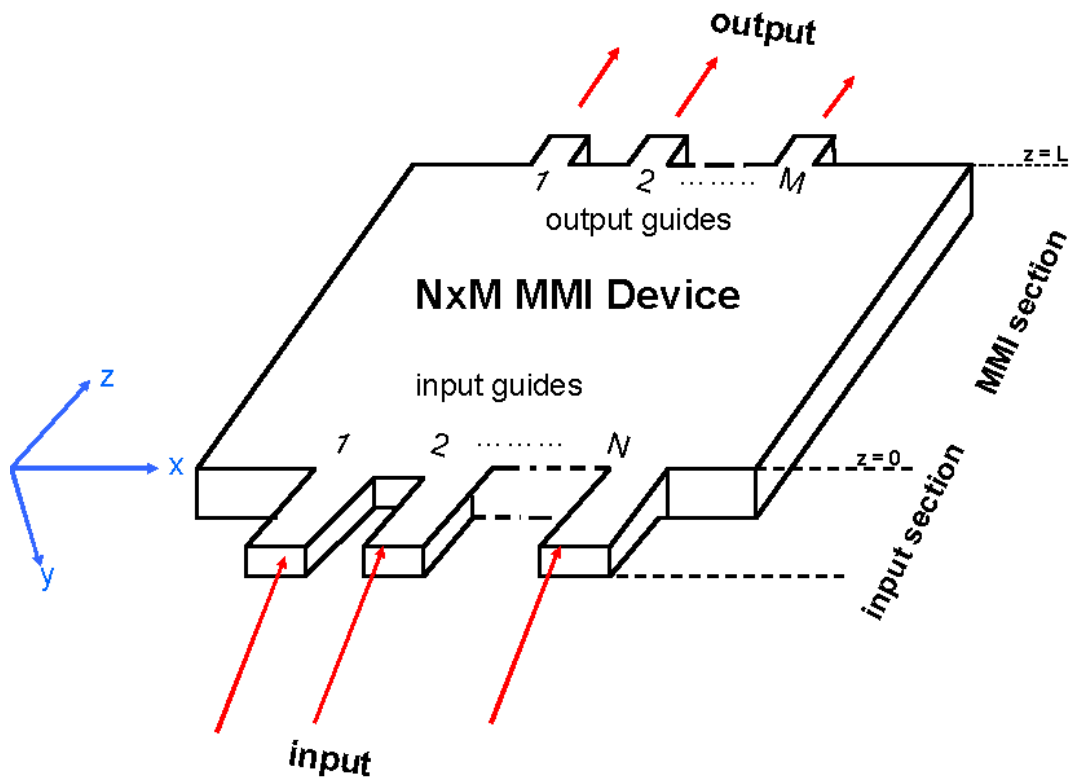


Figure 3.1 Schematic Diagram of $N \times M$ MMI Device.

3.2 Formulation

Solution of wave equation, transcendental equations and propagation constants are shown in appendix-b part of the report. For TE_{mn} and TM_{mn} modes, these equations are given by

$$k_x = \frac{m\pi}{a} \quad n = 0, 1, 2, \dots \quad (3.1)$$

$$k_y = \frac{n\pi}{b} \quad m = 0, 1, 2, \dots \quad (3.2)$$

$$\begin{aligned} \gamma_{mn} &= j\beta_{mn} = j(k_0^2 - k_{c,mn}^2)^{1/2} \\ &= j \left[\left(\frac{2\pi}{\lambda_0} \right)^2 - \left(\frac{m\pi}{a} \right)^2 - \left(\frac{n\pi}{b} \right)^2 \right]^{1/2} \end{aligned} \quad (3.3)$$

For TE modes $m = n = 0$ is the trivial solution, TE_{10} is the fundamental mode. For TM type propagation, TM_{11} is the fundamental mode and indexes (m, n) start from one.

As we can see in Figure 3.1; at $z = 0$ an input field $\Psi(y, 0)$ is applied to the rectangular waveguide. This input field propagates along the rectangular waveguide. When the field comes to the MMI section, higher modes are generated. Each mode has own propagation constant and each mode propagates along the MMI section with a different phase and velocity. At certain distances along the z - axis, these modes are combining. Imaging or reproduction of input field is obtained. In addition to the single images, multiple images can be found as well.

At the beginning of the MMI section, the field will be decomposed into the modal field distributions $\psi_v(x, 0)$ of all modes.

$$\Psi(x, 0) = \sum_v c_v \psi_v(x) \quad (3.4)$$

where the field excitation coefficients c_v can be estimated using overlap integrals

$$c_{mn} = \frac{\int \Psi(x, 0) \psi_{mn}^*(x, y) dx dy}{\int |\psi_{mn}(x, y)|^2 dx dy} \quad (3.5)$$

based on the field-orthogonality relations. $\psi_{mn}^2(x, y)$ is the lateral field profile of the mn^{th} mode.

The field profile at a distance $z = L$ can then be written as a superposition of all the guided (propagated) mode field distributions

$$\Psi(x, y, L) = \sum_{m=1}^M \sum_{n=0}^N c_{mn} \psi_{mn}(x, y) e^{j(\omega t - \beta_{mn} L)} \quad (3.6)$$

where M and N are number of modes.

Assuming the time dependence $e^{j\omega t}$ implicit, we get

$$\Psi(x, y, L) = \sum_{m=1}^M \sum_{n=0}^N c_{mn} \Psi_{mn}(x, y) e^{-j\beta_{mn}L} \quad (3.7)$$

Fundamental mode has the biggest propagation constant, taking the phase of the fundamental mode as a common factor out of the summation.

$$\Psi(x, y, L) = \sum_{m=1}^M \sum_{n=0}^N c_{mn} \Psi_{mn}(x, y) e^{-j\beta_{mn}L} e^{-j\beta_{10}L} e^{j\beta_{10}L} \quad (3.8)$$

$$= e^{j\beta_{10}L} \sum_{m=1}^M \sum_{n=0}^N c_{mn} \Psi_{mn}(x, y) e^{-j\beta_{mn}L} e^{-j\beta_{10}L}$$

$$\Psi(x, y, L) = e^{j\beta_{10}L} \sum_{m=1}^M \sum_{n=0}^N c_{mn} \Psi_{mn}(x, y) e^{j(\beta_{10}-\beta_{mn})L} \quad (3.9)$$

Propagation constants for fundamental TE and TM modes are

$$\beta_{10} = \left[\left(\frac{2\pi}{\lambda_0} \right)^2 - \left(\frac{\pi}{a} \right)^2 \right]^{1/2} \quad \text{for } TE \text{ modes} \quad (3.10)$$

$$\beta_{11} = \left[\left(\frac{2\pi}{\lambda_0} \right)^2 - \left(\frac{\pi}{a} \right)^2 - \left(\frac{\pi}{b} \right)^2 \right]^{1/2} \quad \text{for } TM \text{ modes} \quad (3.11)$$

3.3. Simulation Results

Normalized guided wavelength λ_0/λ_g versus wave number for different modes is shown in figure 3.2.

By defining L_π as the beat length of the two lowest order modes

$$L_\pi = \frac{\pi}{\beta_0 - \beta_1} \quad (3.12)$$

We expect to obtain direct images and multiple images of the input waveform at multiples of beat length.

Dimensions of the input rectangular waveguide are $a=2.2$ cm. $b=1.016$ cm. Width of the MMI section is 6 cm. Operation frequency is selected to be 12 GHz (X – Band). The beat length of the MMI structure is 31.7 cm. We assume that length of the y -axis is very small compared with the width of the MMI section. There is no variation along the y -axis.

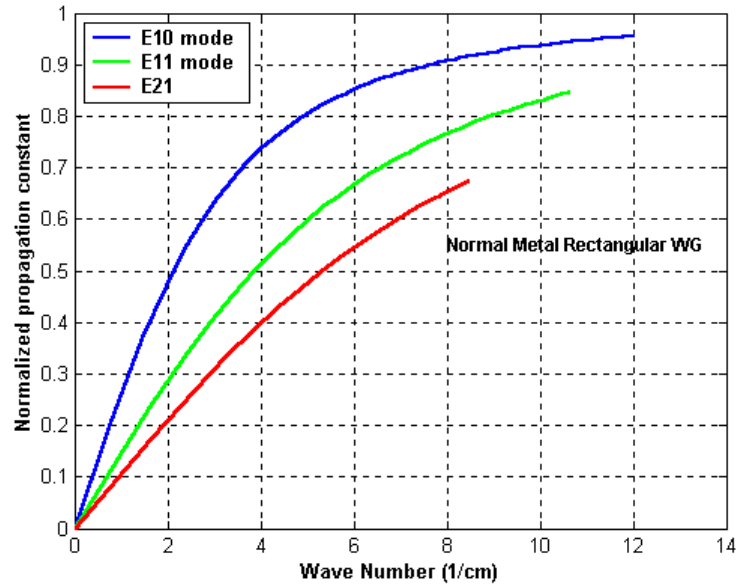


Figure 3.2 Dispersion characteristics of the rectangular waveguide.

In following input-output graphics, the horizontal axis is the x axis (centimeter) and the vertical axis presents the y axis (centimeter) as shown in Figure 3.1.

In figure 3.3, the input-output waveforms at the propagation distance, $L \approx \frac{3}{4}L_\pi$ is given. As expected, input signal is reproduced (self-imaging) at this certain distance.

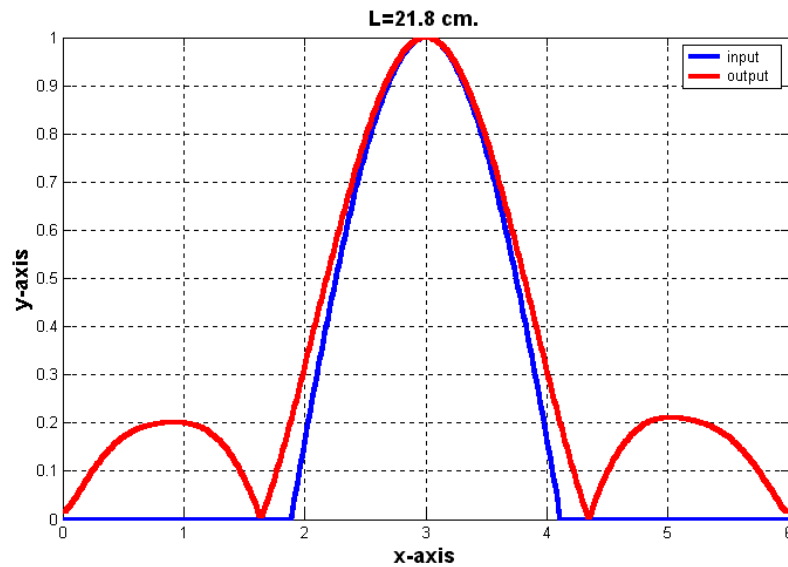


Figure 3.3 Input – output graphic of MMI section at propagation distance $L = 21.8$ cm.

In figure 3.4, direct and mirrored replicas of input waveform at distance $L \approx \frac{3}{8}L_\pi$ is shown. This two-fold imaging could be used to realize 1×2 couplers and splitters.

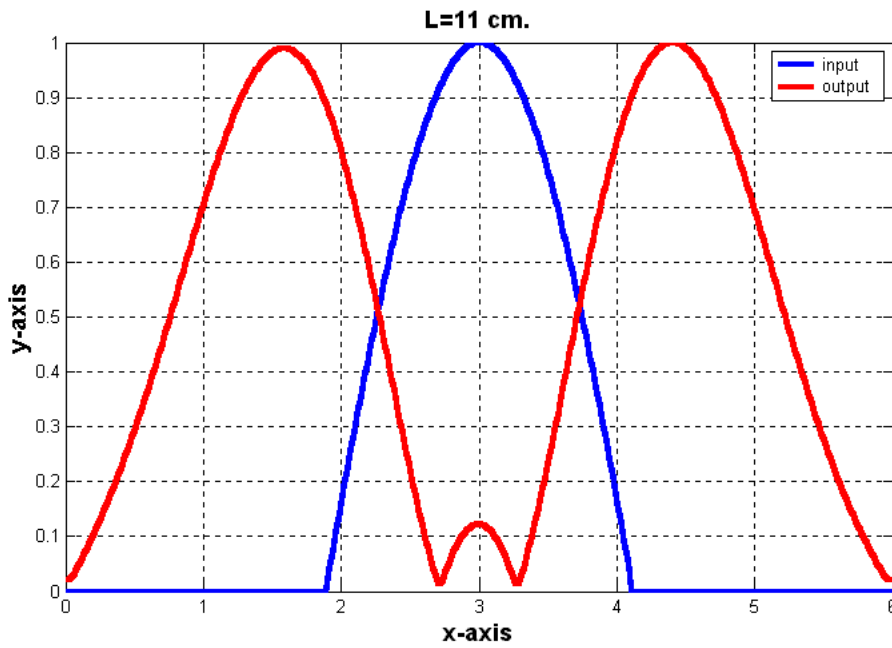


Figure 3.4 Input – output graphic of MMI section at propagation distance $L = 11$ cm.

The multiple self-imaging mechanisms allow the realization of NXN or NXM optical couplers. In figure 3.6, 1×3 MMI coupler has been illustrated.

First single image is obtained at the distance $\frac{3}{4}L_{\pi}$, first N - fold image distance is $\frac{(3L_{\pi})}{4N}$. This information coincides with the Soldano [19].

In figure 3.5, phase characteristics of the input and two-output sections of the 1×2 MMI splitter are illustrated.

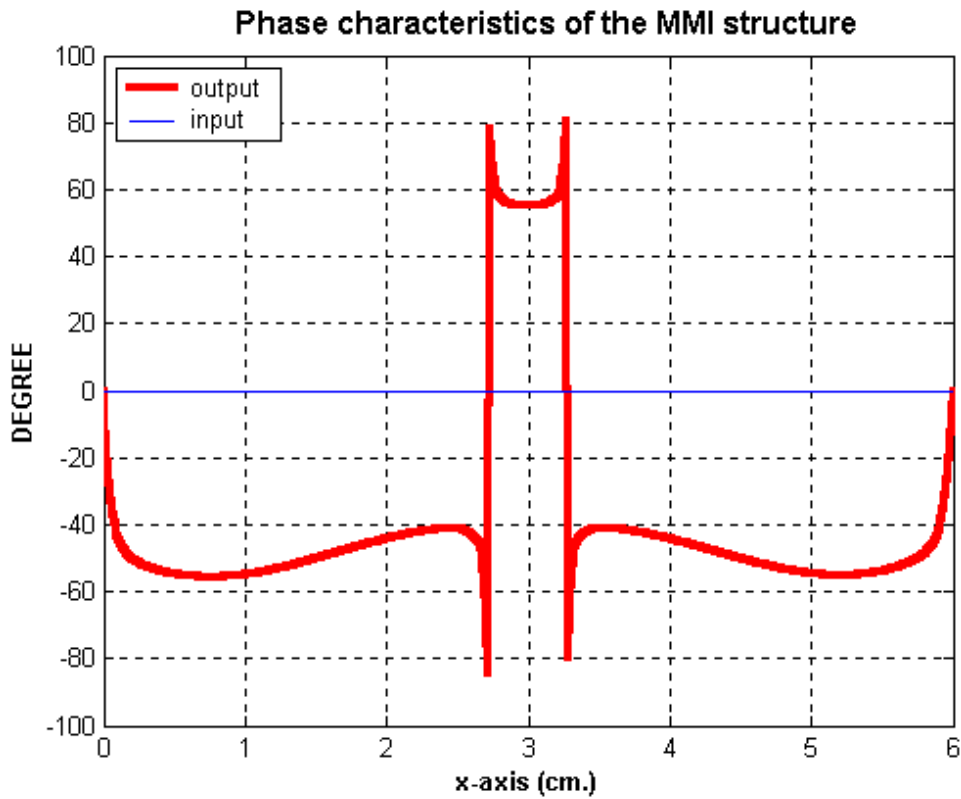


Figure 3.5 Phase characteristics of the MMI structure at propagation distance $L = 11$ cm.

Therefore, we can say that there are no phase differences or phase shifts between two-output ports of the MMI structure.

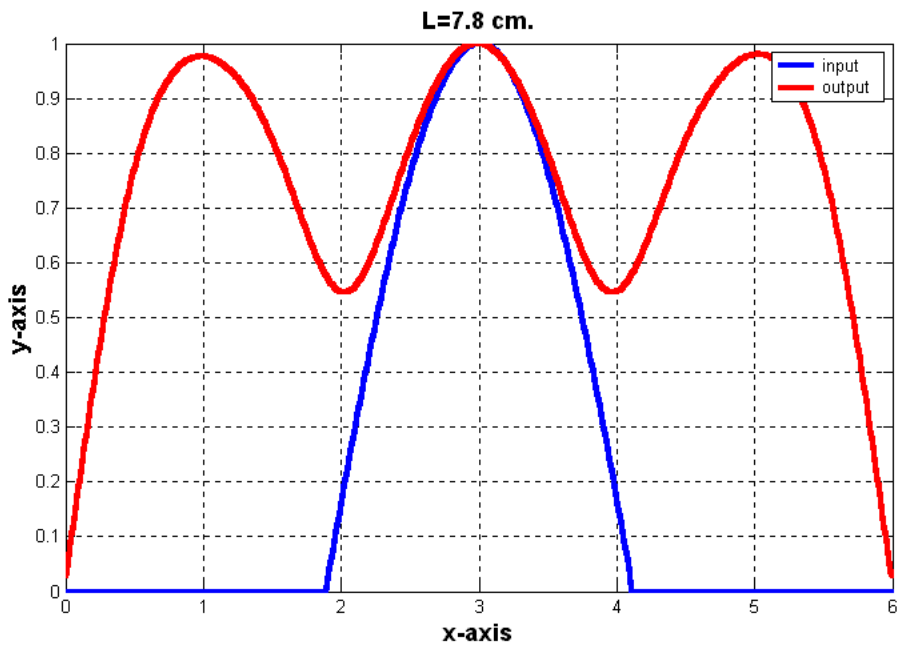


Figure 3.6 Input – output graphic of MMI section at propagation distance $L = 7.8$ cm.

The simulation results show that, the MMI method is a powerful tool to analyze and design rectangular waveguide systems. $N \times M$ MMI couplers, splitter/combiners could be constructed using the MMI method.

Figure 3.7 illustrates the 3-Dimensional representation of 1×2 MMI coupler.

Figure 3.8 shows the first seven propagating modes of the MMI section.

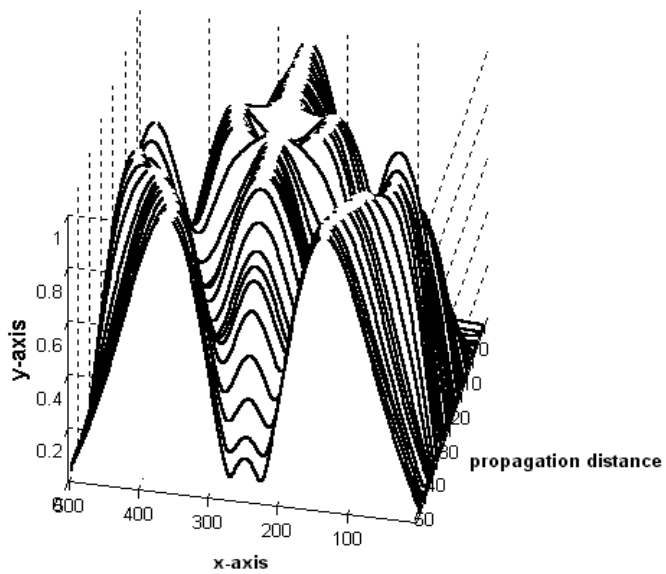


Figure 3.7 3-D simulation of 1x2 MMI coupler.

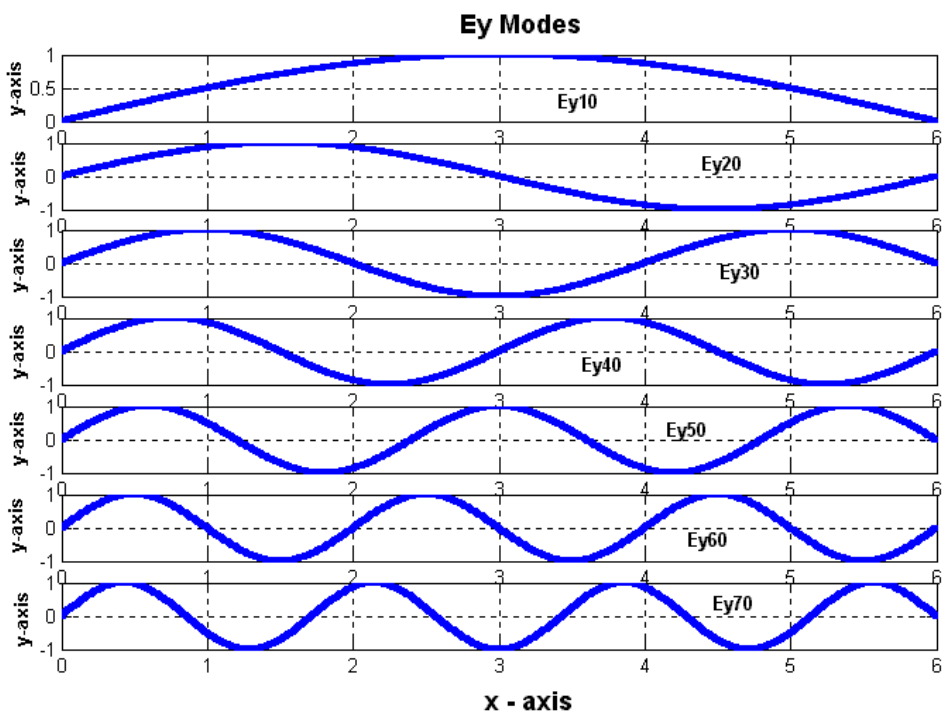


Figure 3.8 First seven E_y propagating modes.

CHAPTER 4

ANALYSIS OF MICROWAVE AND MILLIMETER WAVE DIELECTRIC WAVEGUIDE SYSTEMS

4.1 Introduction

In this chapter the analysis and design of some passive dielectric waveguide devices employing the Multimode Interference Method is presented.

Knox and Toullos have set out the basics of the effective dielectric constant method for simplifying the analysis of related structures [11]. Solbach have improved the formulation [20].

4.2 Formulation

Cross section of image guide is given in Figure 4.1 and the MMI structure is given in Figure 4.2.

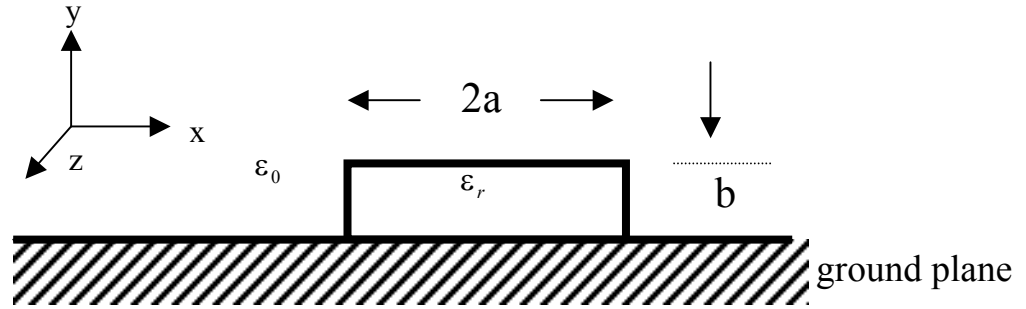


Figure 4.1 Cross section of dielectric image guide.

Transverse propagation constants k_x and k_y in x and y axes are solutions of the following transcendental equations (Appendix C) :

$$ak_x = \frac{m\pi}{2} - \arctan\left(\frac{k_x}{[(\epsilon_{re} - 1)k_0^2 - k_x^2]^{1/2}}\right), \quad m = 1, 2, 3, \dots \quad (4.1)$$

$$bk_y = \frac{m\pi}{2} - \arctan\left(\frac{k_y}{\epsilon_r [(\epsilon_r - 1)k_0^2 - k_y^2]^{1/2}}\right), \quad n = 1, 2, 3, \dots \quad (4.2)$$

k_x is propagation constant in the x direction.

k_y is propagation constant in the y direction.

ϵ_{re} is the effective dielectric constant defined by

$$\epsilon_{re} = \epsilon_r - (k_y/k_0)^2 \quad (4.3)$$

$$k_0 = \frac{2\pi}{\lambda_0} \quad (4.4)$$

λ_0 is free-space wavelength

After determining k_x and k_y ; the propagation constant in z direction is given by the dispersion equation

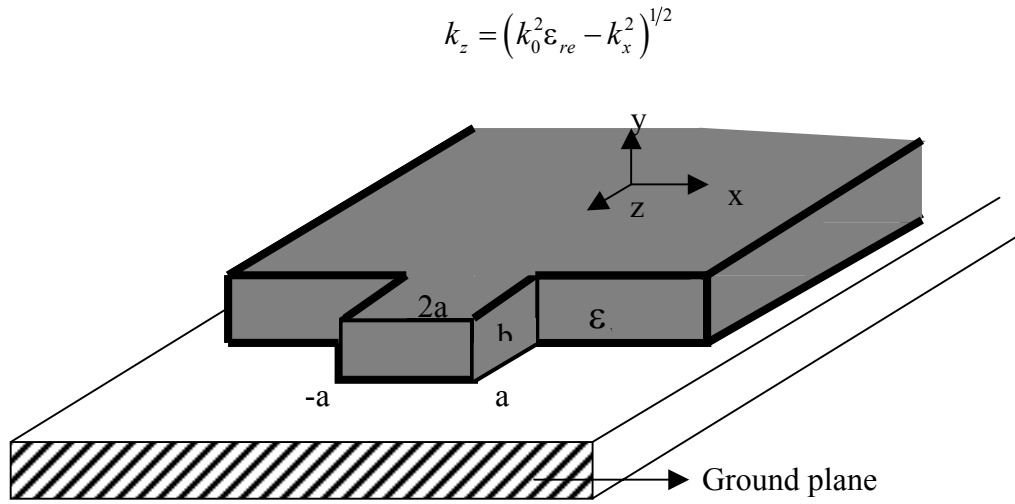


Figure 4.2 3-Dimensional representation of an image guide using MMI approach $2a \gg b$.

Then, using the Multimode Interference Method, the input field is decomposed into modal fields and each one is propagated along the z axis. At a distance, $z = L$ field expression is given by:

$$V_L(z) = e^{jk_1 L} \sum_{m=1}^M c_m v_m(x) e^{-jL(k_1 - k_m)} \quad (4.6)$$

where $v_m(x)$ is the input signal applied to waveguide. c_m is the field excitation coefficient given in equation (2.2).

4.3 Simulation Results

In this section, the simulation results for dielectric slab waveguides obtained using the MMI method are given. Similar to the rectangular waveguides, the input field could be reproduced at certain propagation distances.

Figure 4.3 shows the normalized propagation constants for different modes.

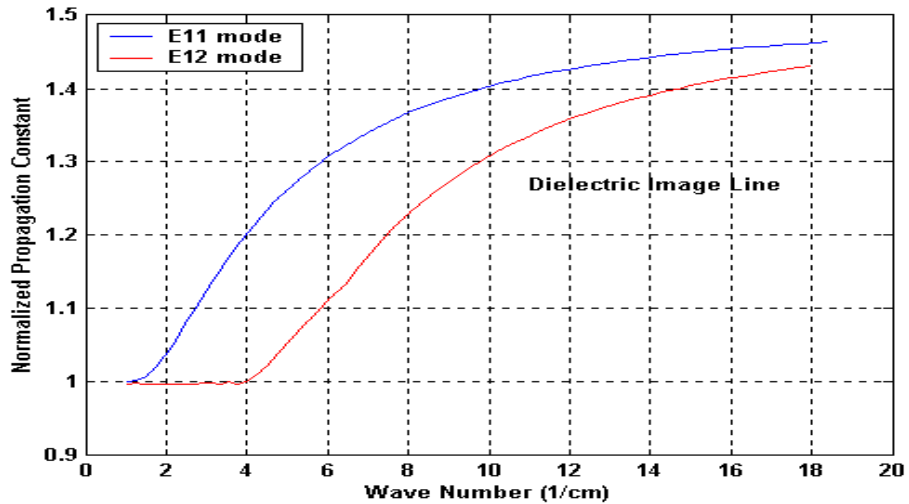


Figure 4.3 A number of modes in the dielectric image line ($2a = 2.2$ cm.
 $b = 0.58$ cm. $\epsilon_r = 4$)

These are simulation results at certain distances, a direct single image of input waveform or a mirrored single image, or N -fold images can be obtained. These propagation distances are related to the beat length of the MMI section and the characteristics (propagation constants, dielectric constant etc.) of the input dielectric waveguide section. Input profile is the fundamental mode $E_{y,11}$.

In following input-output graphics, the horizontal axis is the x axis (centimeter) and the vertical axis presents the y axis (centimeter) as shown in Figure 4.2.

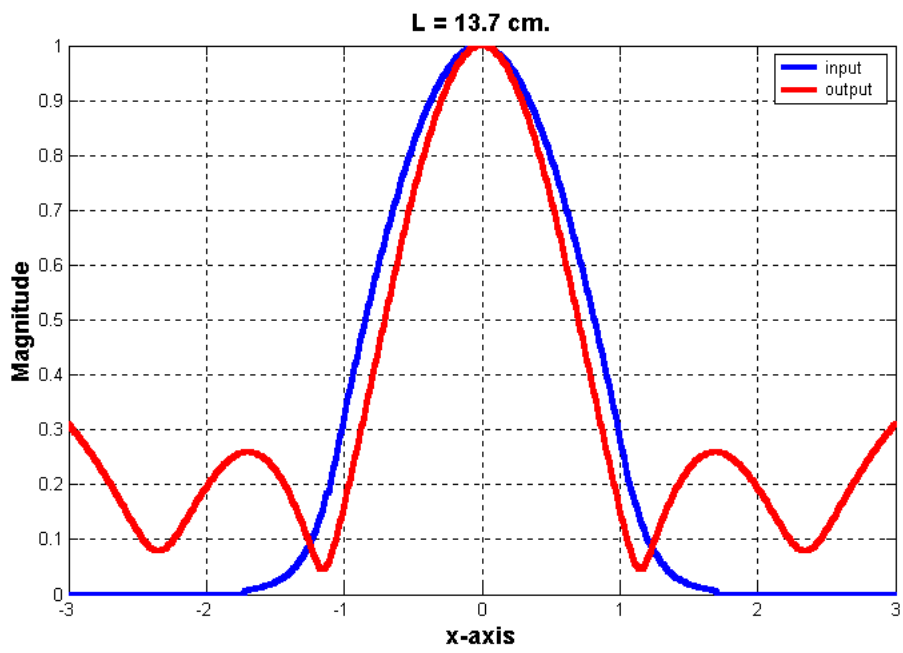


Figure 4.4 Simulation result for propagation distance $L = 13.7$ cm.

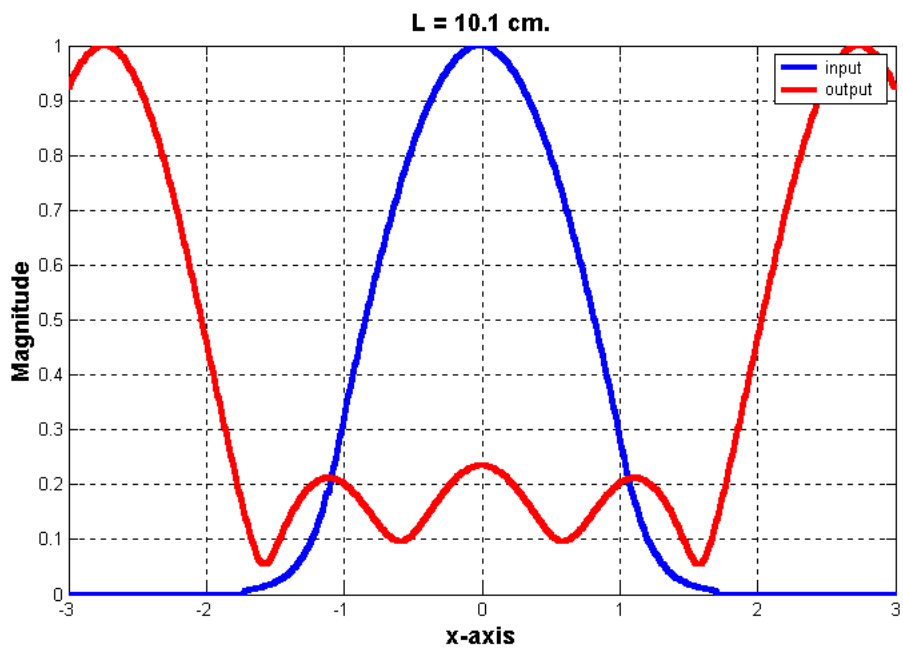


Figure 4.5 Simulation result for propagation distance $L = 10.1$ cm.

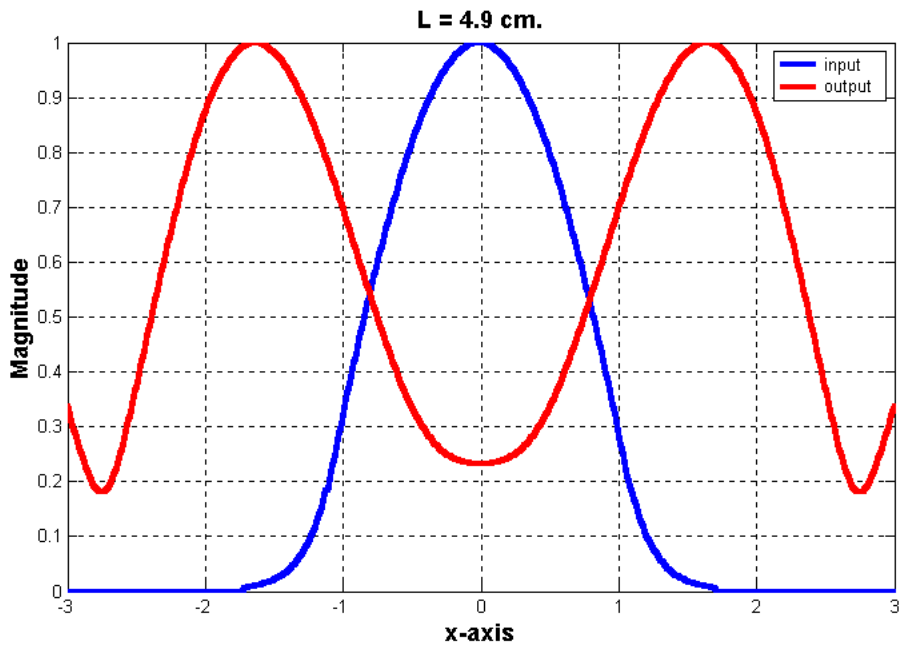


Figure 4.6 Simulation result for propagation distance $L = 4.9$ cm.

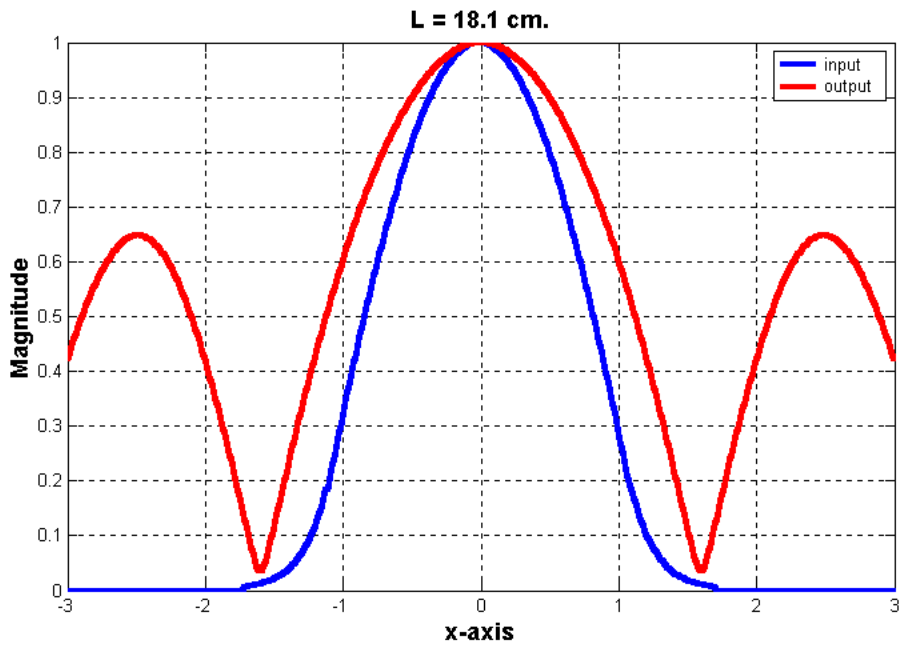


Figure 4.7 Simulation result for propagation distance $L = 18.1$ cm.

In figure 4.8, phase distribution of the 2×2 MMI coupler is illustrated.

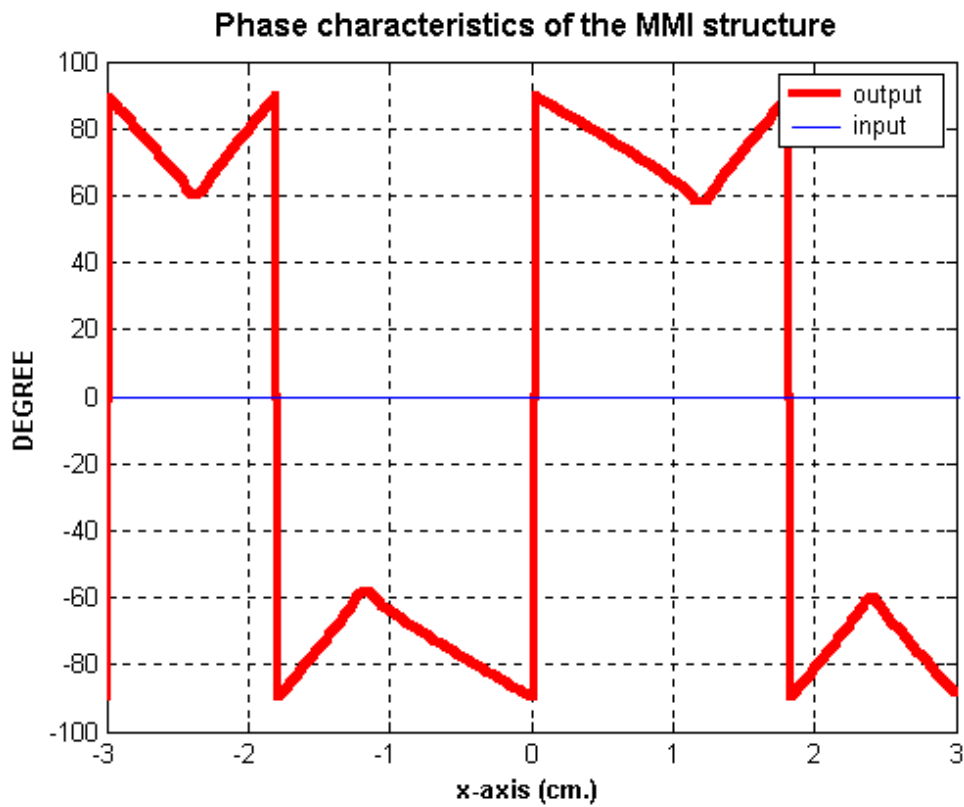


Figure 4.8 Phase characteristics of the input and two-output ports for the dielectric MMI structure.

We can say that, there are no phase differences or phase shifts between two-output ports.

Dimensions of the input dielectric waveguide are $2a=2.2$ cm and $b=1.079$ cm. Operational frequency is chosen $f_0=12$ GHz (X – Band) and the width of the MMI section is 6 cm. Beat length of the structure is $L_\pi=9.3787$ cm. We assume width of the input section is very narrow; there is no variation along the y -axis. Propagation modes are E_{ym1} modes.

First six propagating modes can be seen in figure 4.8

Figure 4.4 shows that, at the propagation distance $L=13.7$ cm. ($L \approx \frac{3}{2}L_\pi$), a single direct replica of the input waveform is obtained. This could be used to design 1×1 MMI coupler.

Figure 4.5 shows that, at the propagation distance $L=10.1$ cm. ($L \approx L_\pi$), a mirrored single image obtained.

Figure 4.6 points out that at the propagation distance $L=4.9$ cm. ($L \approx \frac{1}{2}L_\pi$), two-fold images are obtained. This could be used in the design and analysis of 1×2 MMI coupler.

Figure 4.7 shows that, at the propagation distance $L=18.1$ cm. ($L \approx 2L_\pi$), three-fold image is obtained. This could be used to design and analysis of 1×3 MMI coupler.

In addition to these results, 4-fold images were found at large values of propagation distances.

Figure 4.9 shows the 3-D representation of the 1×2 MMI coupler.

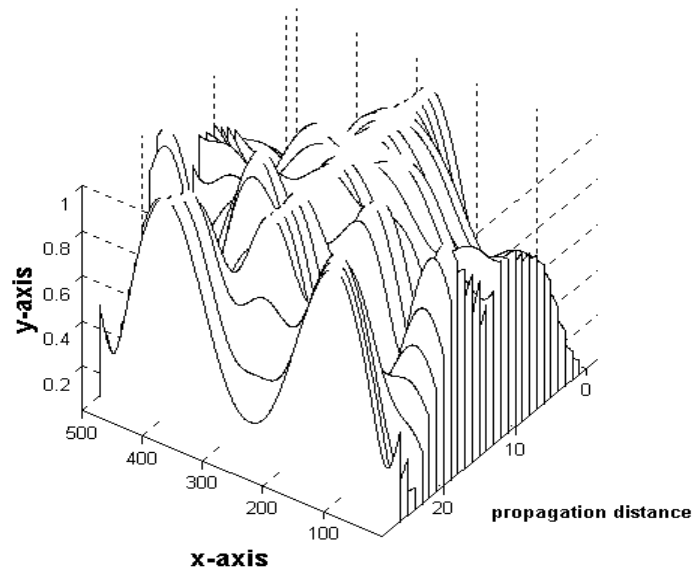


Figure 4.9 3-D plot of the 1x2 MMI coupler.

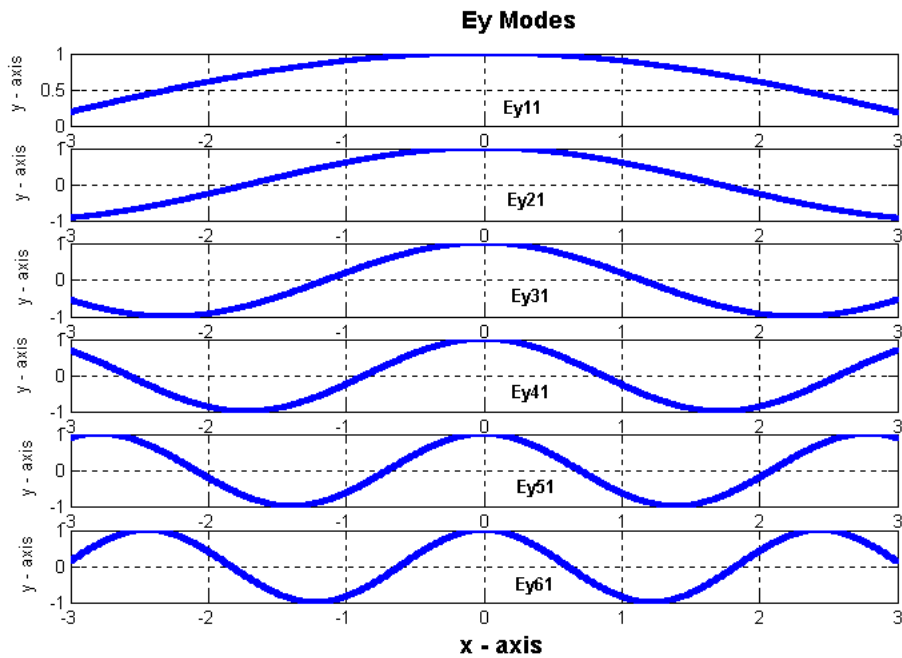


Figure 4.10 First six E_y propagating modes.

Figure 4.10 shows first six propagating modes for the MMI section. Higher modes can propagate in the MMI section but their propagation constants and field excitation coefficients are very small.

The simulation results supports that, the MMI method is a powerful tool for the analysis and the design of the dielectric waveguide systems. $N \times M$ MMI couplers, splitter/combiners could be constructed using the MMI method.

CHAPTER 5

EXPERIMENTAL INVESTIGATION: DESIGN AND CONSTRUCTION OF A MULTIMODED RECTANGULAR WAVEGUIDE SECTION

To investigate the application of the MMI technique experimentally, a metallic waveguide structure operating in the X – band was chosen. The construction of the related structure and the related experimental work are reported in the following sections.

5.1 Construction of the Multimoded H-plane Rectangular Structure

To obtain multimoded operation a stepwise discontinuity in the H-plane was chosen.

The input section is a conventional metallic rectangular waveguide designed for operation at X Band. Following section consists of an H-Plane waveguide whose width is larger than that of the input waveguide section to allow for multimoded propagation.

The conventional waveguide of dimensions 2.25 cm. (width) X 1.016 cm. (height) was joined by the overmoded section of dimension 6 cm. (width) X 1.016 cm. (height) as shown in figure 5.1.

A small vertical E-field probe is used for performing the field amplitude measurements at the aperture of the multimoded section. The length of the structure was chosen to be 34.5 cm. to allow for multiple images in variance cross-sections.

The structure was constructed using the workshop and Millimeter Wave Laboratory facilities at Middle East Technical University, Department of Electrical Electronics Engineering.

5.2 Experiments

Experiments were carried out at the Millimeter wave laboratory of the department of Electrical Electronics Engineering, METU.

An Automatic measurement setup, consisting of Hewlett Packard *8757C Scalar Network Analyzer*, Agilent Technologies *E8257C PSG Analog Signal Generator* and Hewlett Packard *83640A 8360 Series Synthesized Sweeper* was used.

Measurements were carried out at X-band over the frequency range of 8-14 GHz. The input waveguide was excited to support the fundamental TE_{10} mode.

As the aim of the experimental investigations was to study the formation of self and multiple images in the overmoded section, a series of measurements of the electric field profile (E_y component) over the

aperture was made. To make the measurements, a small electric field probe was used.

Measurements were performed at different frequencies ($f = 9, 10, 11, 12, 14$ GHz). The recorded measurement results are given in the following figures together with the theoretical predictions obtained using the formulations presented in Chapter 3.

The reason for carrying out measurements at different frequencies is to be able to investigate the MMI operation for different electrical sizes using the same fixed length overmoded waveguide section.

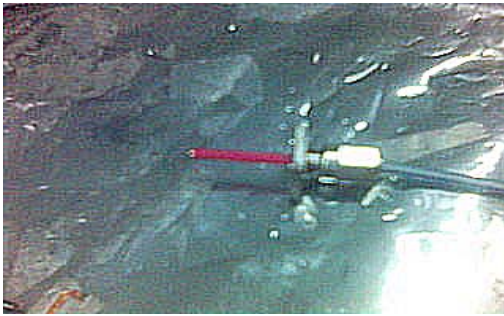
Following figures display the measurement results and theoretical calculations of E-field (E_y components) together to make easier the comparison of the theoretical and experimental results.



(a)



(b)



(c)



(d)



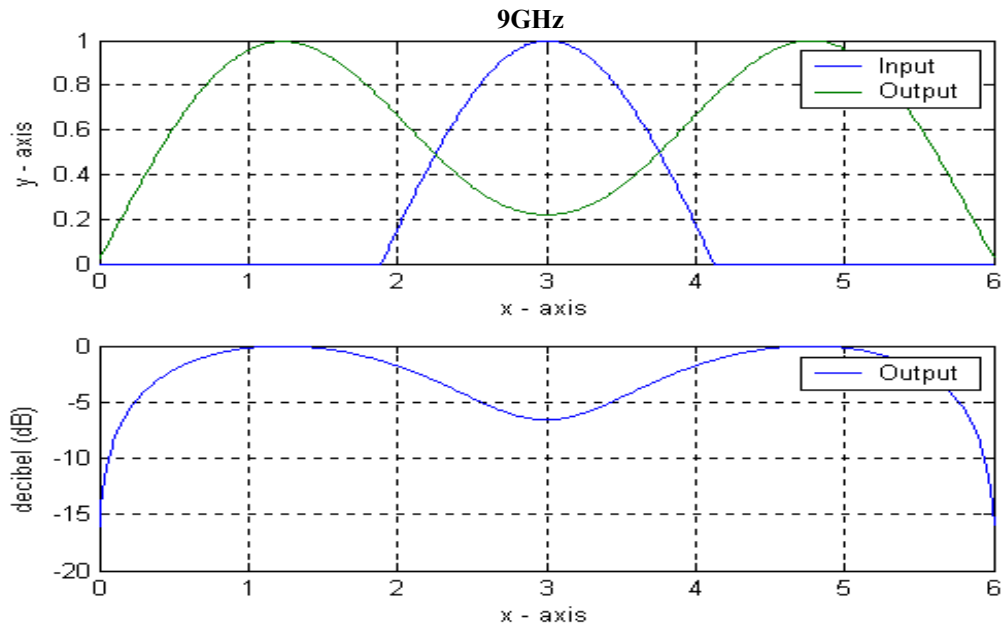
(e)



(f)

Figure 5.1 Experimental setup, (a) input section is a metallic rectangular waveguide, (b) output section, (c) E-field probe, (d) measurement process, (e) MMI section, (f) general structure.

Simulation:



Experimental:

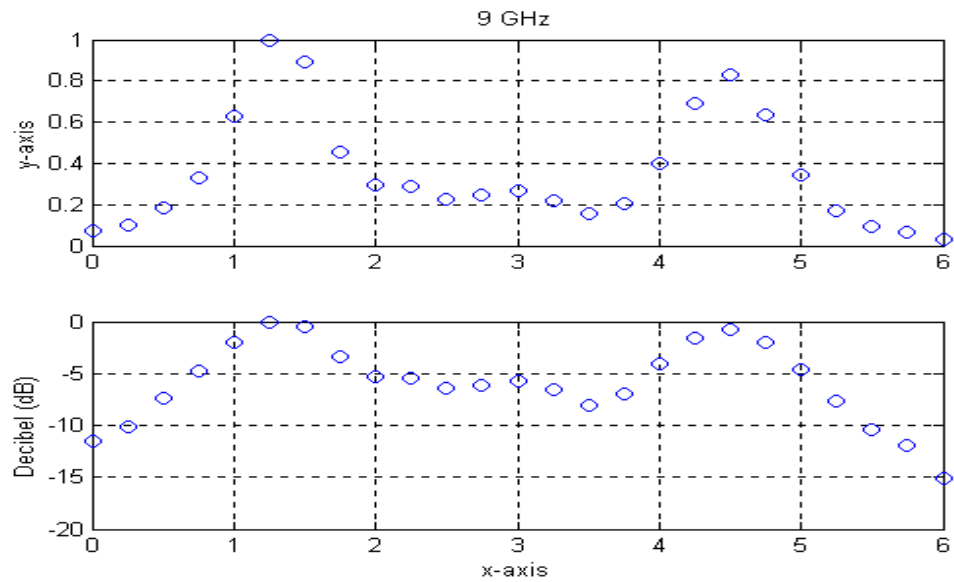
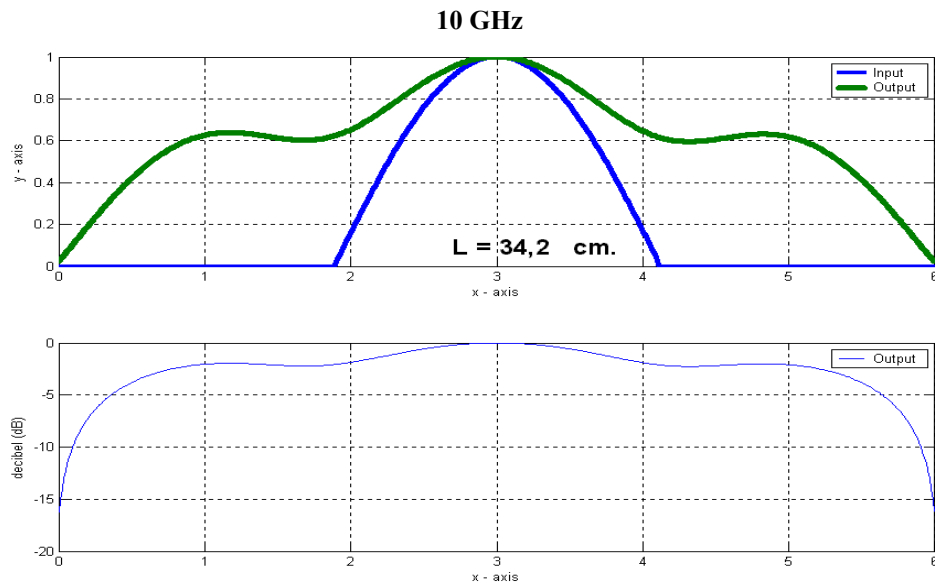


Figure 5.2 Plots of the $|E_y|$ versus distance over the aperture plane with frequency 9 GHz.

Simulation:



Experimental:

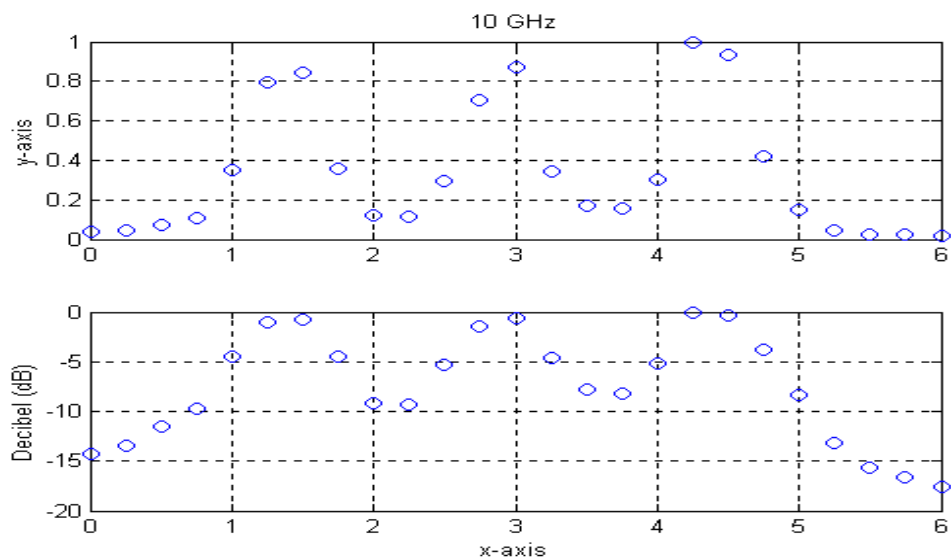
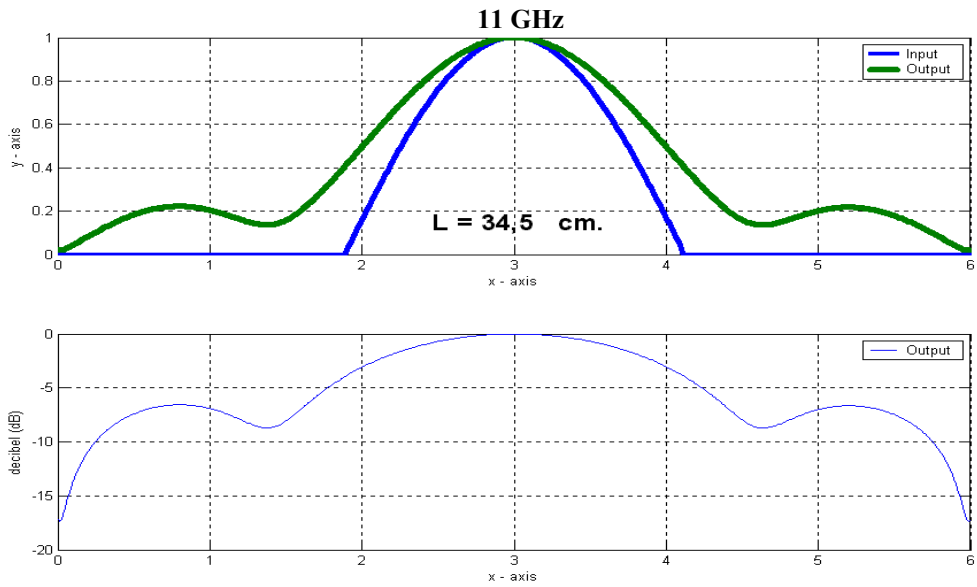


Figure 5.3 Plots of the $|E_y|$ versus distance over the aperture plane with frequency 10 GHz.

Simulation:



Experimental:

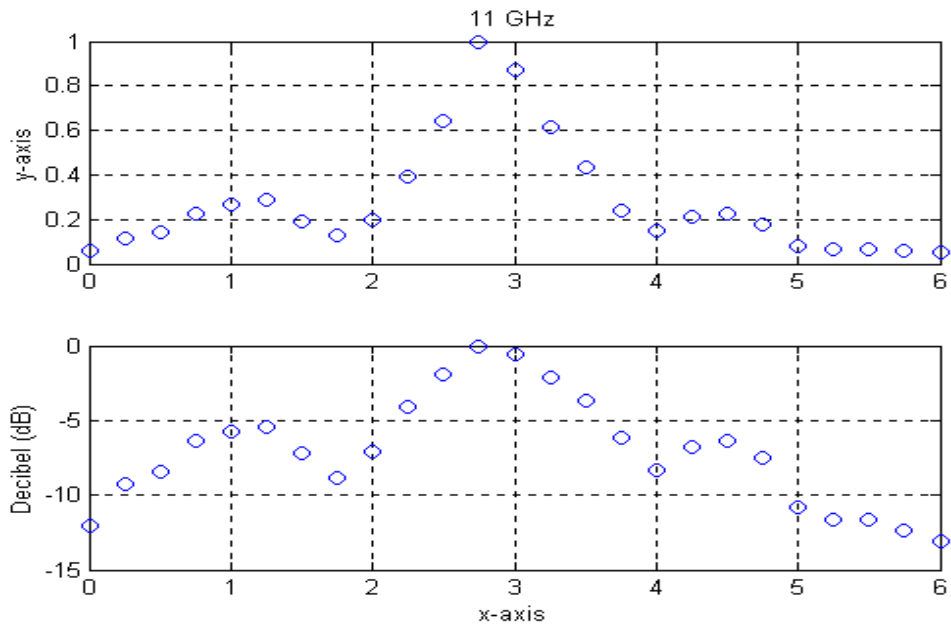
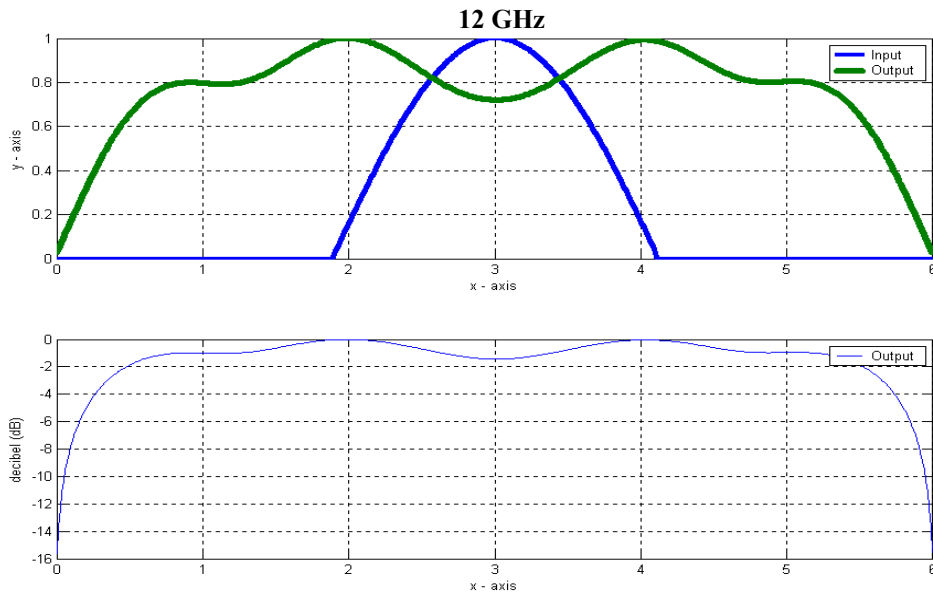


Figure 5.4 Plots of the $|E_y|$ versus distance over the aperture plane with frequency 11 GHz.

Simulation:



Experimental:

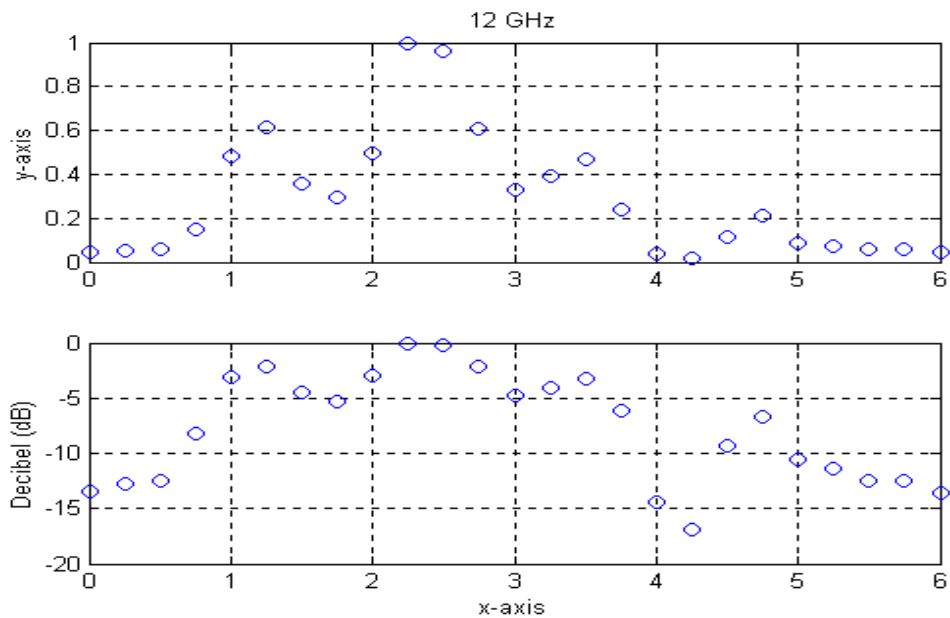
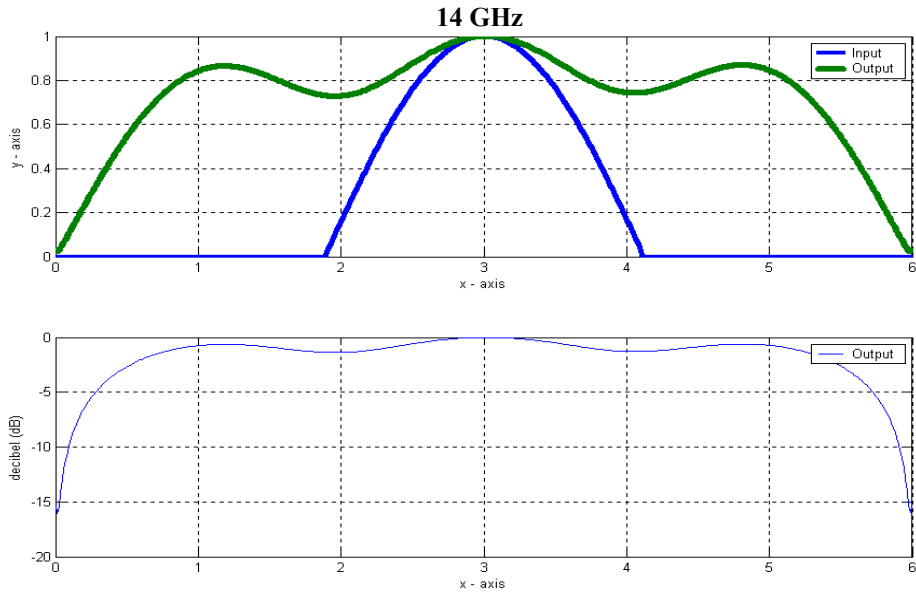


Figure 5.5 Plots of the $|E_y|$ versus distance over the aperture plane with frequency 12 GHz.

Simulation:



Experimental:

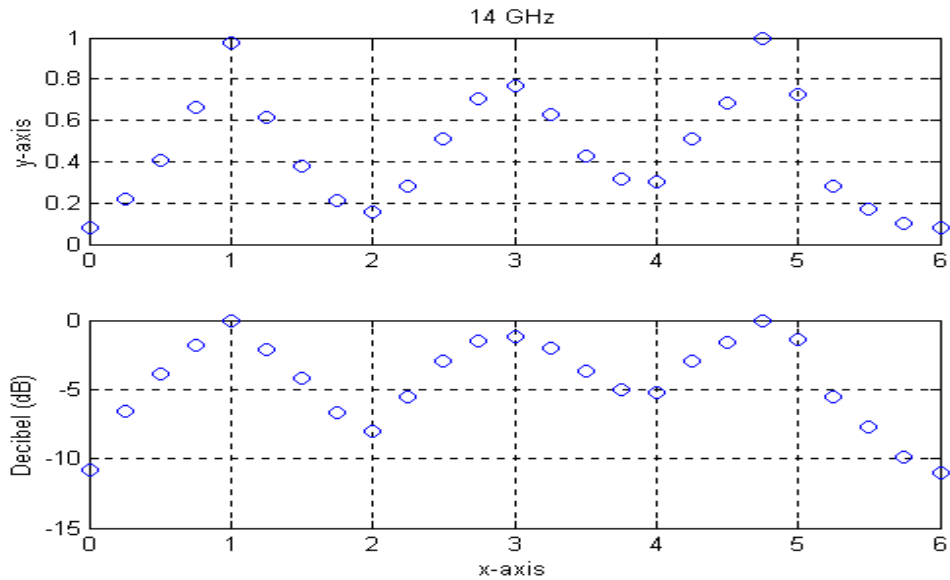


Figure 5.6 Plots of the $|E_y|$ versus distance over the aperture plane with frequency 14 GHz.

5.3 Discussions

Using the 2-section WG jig, the concept of self and multiple imaging was also verified experimentally. The general features of the measurement with the simulation results show agreement. However, the measuring probe together with the associated mount (connector and wiring) has an appreciable size and therefore may cause distortion of the true field distribution. In addition the positioning mechanism is not precise. Therefore these factors obviously caused experimental errors. Yet, it can be said that the experimental program has achieved its goal of demonstrating the "imaging property".

Thus the experimental investigations have revealed that the MMI method can be used in the analysis and design of passive microwave and millimeter wave devices as well as optical systems or system components.

CHAPTER 6

CONCLUSIONS

In this thesis, we investigated the self-imaging principle and multimode interference (MMI) mechanism and introduced the integrated optical devices based on multimode interference. Previously, Soldano reported on the fabrication of a series of 2×2 MMI coupler and 1×2 MMI splitters [13],[14]. Based on his work, in the first step of our study we performed the computer simulations for these MMI devices.

Moreover, in this thesis our aim was to analyze overmoded 'rectangular metallic' and 'dielectric slab' type of waveguides and devices, which are widely used in telecommunication systems, using the MMI approach. In addition to the computer simulations, we employed an experimental setup to investigate the application of the MMI technique to such devices. The results of the experiments showed that, the MMI method is a powerful tool in the design of millimeter wave waveguides and devices.

Making use of the formulations and simulations developed in this thesis, further studies can be undertaken to develop new types of beam forming networks. The final output sections of the MMI devices, shown in Figure 3.1, may consist of horn antennas. Thus, one can realize the design of an antenna array feed network using this approach.

REFERENCES

- [1] H.F. Talbot, "Facts relating to optical science No. IV." *The London and Edinburgh Philosophical Magazine and Journal of Science*, vol. 9, pp. 401-407, December 1836. Third Series.
- [2] D.. Marcuse, *Light Transmission Optics*. New York: Van Nostrand Reinhold. 1972.
- [3] O. Bryngdahl, "Image formation using self-imaging techniques," *J. Opt. Soc. Am.*, vol. 63, no. 4, pp. 416-419, 1973.
- [4] R. Ulrich, "Image Formation by phase coincidences in optical waveguides." *Optics Communications*, vol. 13, no. 3, pp. 259-264, 1975.
- [5] R. Ulrich, "Light-propagation and imaging in planar optical waveguides," *Nouv. Rev. optique*, vol. 6, no. 5, pp. 253-262, 1975.
- [6] C. vazquez, F. J. Mustielea and F. Hernandez-Gil, "Three-Dimensional Method for Simulation of Multimode Interference Couplers," *Journal of Lightwave Technology*, vol. 13, no. 11, pp. 2296-2299, 1995.
- [7] W. C. Ng, M. S. Stern, "Analysis of Multiple-Rib Waveguide Structures by the Discrete-Spectral-Index Method," *IEE Proc. on Optoelectron*. Vol. 145, no. 6, pp. 365-371, 1998.
- [8] P. N. Robson and P. C. Kendall, eds., "Rib waveguide theory by the spectral index method." *Optoelectronic Series*, John Wiley & Sons Inc. 1990.
- [9] P. A. Besse, M. Bachmann, H. Melchior, L.B. Soldano, M.K. Smit, "Optical bandwidth and fabrication tolerances of multimode interference couplers", *Journal of Lightwave Technology*, vol. 12, Issue 6, pp. 1004 – 1009, 1994.
- [10] Lucas Beda Soldano, "Multimode Interference Couplers Design and Application", Delfth University of Technology Phd thesis, 1994.
- [11] R. M. Knox and P.P. Toullos, "Integrated circuits for the millimeter through optical frequency range," in *Proc. MRI Symp. On Submilimeter Waves* (J. Fox, ed.), (New York, USA), pp. 497-516, Polytechnic Press, 1970.
- [12] R. Ulrich, "Image Formation by Phase Coincidences in Optical Waveguides," *Optics Communications*, vol. 13, no. 3, pp. 259-264, 1975.

- [13] Lucas B. Soldano, Frank B. Veerman, M. K. Smit, Bastiaan H. Verbeek, Alain H. Dubost and Eric C. M. Pennings, "Planar Monomode Optical Couplers Based on multimode Interference Effects," *Journal of Lightwave Technology*, vol. 10, no. 12, pp. 1843-1850, 1992.
- [14] E. C. M. Pennings, R. J. Deri, A. Scherer, R. Bhat, T. R. Hayes, n. C. Andreadakis, M. K. Smit, L. B. Soldano, and R. J. Hawkins, "Ultracompact, Low-loss Directional Couplers on InP based Self-Imaging by Multimode Interference," *Applied Phys. Letters*, vol. 59, no. 16, pp. 1946-1928, 1991.
- [15] A. Ferreras, F. Rodriguez, E. Gomez-Salas, J. L. de Miguel, and F. Hernandez-Gil, "Useful Formulas for Multimode Interference Power Splitter/Combiner Design," *IEEE Photonics Technology Letters*, vol. 5, no. 10, 1993.
- [16] James A. Besley, John D. Love and Wendy Langer, "A Multimode Planar Power Splitter," *Journal of Lightwave Technology*, vol. 16, no. 4, pp. 678-684, 1998.
- [18] R. E. Collin. "Foundations for Microwave Engineering." McGraw-Hill, Inc., 1966.
- [17] Constantine A. Balanis. "Advanced Engineering Electromagnetics." John Wiley and Sons, Inc., 1989.
- [19] Lucas B. Soldano and Erik C. M. Pennings, "Optical Multi-Mode Interference Devices Based on Self-Imaging: Principles and Applications." *Journal of Lightwave Technology*, vol. 13, no. 4, pp 615-627, 1995.
- [20] Klaus Solbach, "The Calculation and the Measurement of the Coupling Properties of Dielectric Image Lines of Rectangular Cross Section," *IEEE Transactions on Microwave Theory and techniques*, vol. MTT-27, no. 1, pp.54-58, 1979.
- [21] E. A. J. Marcatili, "Dielectric Rectangular Waveguide and Directional Couplers for Integrated Optics", *Bell System Technical Journal*, vol. 48, no. 7, 1969, pp. 2071-2102.
- [22] J. leuthold, J. Eckner, Emil Gamper, Pierre A. Besse, and Hans Melchior, "Multimode Interference Couplers for the Conversion and Combining of Zero- and First-Order Modes, *Journal of Lightwave Technology*, vol. 16, no. 7, 1998.
- [23] R. M. Lorenzo, C. Ilorente, E. J. Abril, M. Lopez, "Improved Self-Imaging Characteristics in 1 X N Multimode Couplers," *IEE Proc.-Optoelectron.*, vol. 145, no. 1, pp. 65-69, 1998.
- [24] S. Nagai, Goh Morishima, H. Inayoshi, and Katsuyuki Utaka, "Multimode Interference Photonic Switches," *Journal of Lightwave Technology*, vol. 20, no. 4, 2002.

- [25] M. Shamonin, M. Lohmeyer and P. Hertel, "Directional Coupler Based on Radiatively Coupled waveguides," *Department of Physics , University of Osnabrück Barbaratraße 7, D-49069 Osnabrück, Germany*,1995.
- [26] Thua Van Ho and John Litva, "Adaptive Beamforming Using Multimode Feed Horn Antennas," pp. 1654-1657, ISDN: CH2654-2/59/0000-1654,2002.
- [27] John J. Kenny, "Multimode Interference Generation in the Horn-reflector Antenna System During Multipath Fading," pp. 42-47, ISDN: CH2682-3/89/0000-0042,1989.
- [28] E. C. Pennings, R. van roijen, M. J. N. van Stralen, P. J. de Waard, r. G. M. P. Koumans and B. H. Verbeek. "Reflection Properties of Multimode Interference Devices," *IEEE Photonics Technology Letters*, vol. 6, no. 6, 1994.
- [29] Qian Wang, jun Lu, Sailing He, "Optimal Design of a Multimode Interference Coupler Using a Genetic Algoritm," *Optics Communication* vol. 20, no. 9, pp. 131-136, 2002.
- [30] Marek Blahut, P. Karasinski, D. Kasprzak, Roman Rogozinski, "Visualization Method of Modal Interference in Multimode Interference Structures," *Optics communications*, vol. 21, no. 4, pp. 47-53, 2002.
- [31] J. R. Pujol Poa, W. Biehlig, and F. Lederer, "A Generalization of the Spectral Index Method Toward Multiple Rib Waveguides," *Journal of Lightwave Technology*, vol. 14, no. 3, pp. 454-461, 1996.
- [32] Olof Bryndahl, "Image Formation Using Self-Imaging Techniques," *Journal of the Optical Society of America*, vol. 63, no. 4, pp 416-419, 1973.
- [33] R. Ulrich and G. Ankele, "Self-Imaging in Homogeneous Planar Optical Waveguides," *Applied Physics Letters*, vol. 27, No. 6, pp. 337-339, 1975.
- [34] M. S. Stern, P. C. Kendall, P. W. A. Mcllroy, "Analysis of the Spectral Index Method for Vector Modes of Rib Waveguides," *IEE Proceedings*, vol. 137, Pt. J, no. 1, pp. 21-26, 1990.
- [35] Mohamad Deeb, Abouzahra, and Leonard J. Ewin, "Coupling of Degenerate Modes on Curved Dielectric Slab Sections and Application to Directional Couplers," *IEEE Transactions on Microwave Theory and Techniques*, vol. MTT-28, no. 10, pp. 1096-1101, 1980.
- [36] Ayman Yehia and Diao Khalil, "Analysis of 2D Multimode Interference Structures," ISDN: 0-7803-7556-4/02, 2002 IEEE.
- [37] M. Tuncay Birand, "A Novel Frequency Scanning Millimeter Wave Array," *METU Journal of Pure and Applied Sciences*, vol. 16, no. 1, pp. 111-134, 1983.

- [38] William V. McLevige, Tatsuo Itoh, and Raj Mittra, "New Waveguide Structures for Millimeter-Wave and Optical Integrated Circuits," *IEEE Transactions on Microwave Theory and Techniques*, vol. MTT-23, no. 10, pp. 788-794, 1975.
- [39] A. Simon and R. Ulrich, "Fiber-optical Interferometer," *Applied Phys. Lett.*, vol. 31, no. 2, pp. 77-79, 1977.
- [40] O. Zhuromskyy, M. Lohmeyer, N. Bahlmann, P. Hertel, H. Dötsch, "Analysis of Nonreciprocal Light Propagation in Multimode Imaging Devices," *Zelenograd Research Institute of Physical Problems*, pp. 1-11, 1998.
- [41] Paul W. A. McIlroy, Michael S. Stern, and Peter C. Kendall, "Spectral Index method for Polarized Modes in Semiconductor Rib Waveguides," *Journal of Lightwave Technology*, vol. 8, no. 1, pp. 113-17, 1990.
- [42] Y. Kawaguchi and K. Tsutsumi, "Mode Multiplexing and Demultiplexing Devices Using Multimode Interference Couplers," *Electronics Letters*, vol. 38, no. 25, 2002.
- [43] John M. Heaton, and R. Michael Jenkins, "General Matrix Theory of Self-Imaging in Multimode Interference (MMI) Couplers," *IEEE Photonics Technology Letters*, vol. 11, no. 2, pp. 212-214, 1999.
- [44] Hongzhen Wei, Jinzhong Yu, Xiaofeng Zhang, Wei Shi, and Changshui Fang, "Signal bandwidth of General $N \times N$ Multimode Interference Couplers," *Journal of Lightwave Technology*, vol. 19, no. 5, pp. 739-745, 2001.
- [45] Juerg Leuthold, and Charles H. Joyner, "Multimode Interference Couplers with Tunable Power Splitting Ratios," *Journal of Lightwave Technology*, vol. 19, no. 5, pp. 700-707, 2001.
- [46] B. M. A. Rahman, M. Rajarajan, T. Wongcharoen, and K. T. V. Grattan, "Accurate Analysis of Multimode Interference Devices," *IEEE Photonics Technology Letters*, vol. 8, no. 6, pp. 809-811, 1996.

APPENDIX A

ANALYSIS OF OPTICAL SLAB WAVEGUIDES

A.1 Theoretical Background

The electric field intensity vector \vec{E} and electric displacement vector \vec{D} are related to the magnetic field intensity vector \vec{H} and the magnetic flux density vector \vec{B} by the Maxwell's equations. Field vectors that vary with space coordinates and are sinusoidal functions of time can similarly be represented by vector phasors that depend on space coordinates but not on time. As an example, we can write a time-harmonic \vec{E} field referring to $\cos(\omega t)$ as follows

$$\vec{E}(x, y, z, t) = \Re \left[\vec{E}(x, y, z) e^{j\omega t} \right] \quad (\text{A.1})$$

where $\vec{E}(x, y, z)$ is a vector phasor that contains information on direction, magnitude, and phase.

Time-harmonic Maxwell's equations in terms of vector field phasors (\vec{E}, \vec{H}) and source phasors (ρ, J) in a linear, isotropic and homogeneous medium as follows

$$(\text{A.2})$$

$$\begin{aligned}\nabla \times \bar{H} &= \bar{J} + j\omega\varepsilon\bar{E} \\ \nabla \times \bar{E} &= -j\omega\mu\bar{H}\end{aligned}\tag{A.3}$$

$$\nabla \cdot \bar{E} = \rho/\varepsilon\tag{A.4}$$

$$\nabla \cdot \bar{H} = 0\tag{A.5}$$

where ε is dielectric permittivity and μ is known as the magnetic permeability of the medium.

A.2 Wave Optics: Solutions of Wave Equation

A.2.1 Introduction

The important wave equation, which is used in the MMI method, is described. After applying this basic equation to slab waveguide, the eigenvalue equations are calculated for TE and TM modes. Finally an approximation method to solve this eigenvalue equations are generated for even, odd TE and TM modes in the last part of chapter.

D. Marcuse investigated the light propagation in optical waveguides [2]. Wave optics is directly based on Maxwell's equations to solve problems of light propagation, while ray optics uses the short wavelength of light to simplify many problems of light propagation. Ray optics is similar to the mechanics of point particles in many ways, while wave optics corresponds to the quantum theory of light rays.

A.2.2 Wave Equation

Electric field intensity vector depends on magnetic flux density vector by the equation

$$\nabla \times \bar{E} = -\frac{\partial \bar{B}}{\partial t} - \bar{J} \quad (\text{A.6})$$

where

$$\bar{B} = \mu \bar{H} \quad (\text{A.7})$$

Substitute (A.7) into (A.6) and take the curl of this latter equation.

$$\nabla \times (\nabla \times \bar{E}) = -\mu \frac{\partial}{\partial t} (\nabla \times \bar{H}) \quad (\text{A.8})$$

In deriving of equation (A.8) it is assumed that μ is a constant and independent of the space coordinates. Curl of the magnetic field intensity vector \bar{H} depends on the electric displacement vector \bar{D} ; also $\bar{D} = \epsilon \bar{E}$ is given. Substitution of these relationships into (A.8), yields an equation which depends only on the vector \bar{E} itself

$$\nabla \times (\nabla \times \bar{E}) + \epsilon \mu \frac{\partial^2 \bar{E}}{\partial t^2} = 0 \quad (\text{A.9})$$

This equation holds even if ϵ varies in space.

The $\nabla \times \nabla \times$ operator is not very easy to use, so that it is advantageous to introduce the vector identity

$$\nabla \times (\nabla \times \bar{E}) = \nabla (\nabla \cdot \bar{E}) - \nabla^2 \bar{E} \quad (\text{A.10})$$

which holds if we use a Cartesian coordinate system. Using $\bar{D} = \epsilon \bar{E}$

$$\nabla^2 \bar{E} + \nabla \left(\bar{E} \cdot \frac{\nabla \epsilon}{\epsilon} \right) = \epsilon \mu \frac{\partial^2 \bar{E}}{\partial t^2} \quad (\text{A.11})$$

In the special case that ϵ is constant in space, the gradient of the ϵ vanishes, and equation (A.11) assumes the form of the wave equation

$$\nabla^2 \bar{E} = \epsilon \mu \frac{\partial^2 \bar{E}}{\partial t^2} \quad (\text{A.12})$$

Using phasor notation and Fourier Integration, the integral representation of the most general wave propagating in a dispersive medium is given

$$f(x, y, z, t) = \frac{1}{4\pi^3} \int_0^\infty d\omega \int_{-\infty}^\infty dk_x \int_{-\infty}^\infty dk_y \left| \phi(k_x, k_y, \omega) \right| \cos(\omega t - k_x x - k_y y - k_z z + \theta) \quad (\text{A.13})$$

For analyzing optical systems, method of normal modes is used. When ϵ is a function of space coordinates, the superposition of plane waves is no longer a solution of the wave equations.

The definition of modes is quietly simple. A mode is a solution of eigensolution of Maxwell's equations under specific boundary conditions of the problem. Electrical and Magnetic field expressions are written as

$$\bar{E} = A e^{j[(\omega t - \bar{k} \cdot \bar{r})]} \bar{e} \quad (\text{A.14})$$

$$\bar{H} = B e^{j[(\omega t - \bar{k} \cdot \bar{r})]} \bar{h} \quad (\text{A.15})$$

where A and B are complex coefficients. \bar{e} and \bar{h} are unit vectors.

We must satisfy the Maxwell's equations.

$$(\text{A.16})$$

$$\begin{aligned}
-j(\bar{k} \times \bar{h})B &= j\omega\epsilon A\bar{e} \\
-j(\bar{k} \times \bar{e})A &= j\omega\mu B\bar{h}
\end{aligned} \tag{A.17}$$

Boundary conditions, which must be satisfied, are following

$$\bar{n} \cdot \bar{e} = 0 \tag{A.18}$$

$$\bar{h} = \bar{n} \times \bar{e} \tag{A.19}$$

$$B = \sqrt{\frac{\epsilon}{\mu}} A \tag{A.20}$$

We can try to find mode solutions of the following mode form

$$\bar{E} = E_0(x, y)e^{[j(\omega t - \beta z)]} \tag{A.21}$$

$$\bar{H} = H_0(x, y)e^{[j(\omega t - \beta z)]} \tag{A.22}$$

Substitution of these equation into (A.2) and (A.3) with the help of (A.7) and $\bar{D} = \epsilon\bar{E}$; following sets of equations are found

$$\frac{\partial H_z}{\partial y} + j\beta H_y = j\omega\epsilon E_x \tag{A.23}$$

$$-j\beta H_x - \frac{\partial H_z}{\partial x} = j\omega\epsilon E_y \tag{A.24}$$

$$\frac{\partial H_y}{\partial x} - \frac{\partial H_x}{\partial y} = j\omega\epsilon E_z \tag{A.25}$$

$$\frac{\partial E_z}{\partial y} + j\beta E_y = -j\omega\mu H_x \tag{A.26}$$

$$j\beta E_x + \frac{\partial E_z}{\partial x} = j\omega\mu H_y \tag{A.27}$$

$$\frac{\partial E_y}{\partial x} - \frac{\partial E_x}{\partial y} = -j\omega\mu H_z \tag{A.28}$$

Using (A.23), (A.24), (A.26) and (A.27); the transverse field components could be expressed in terms of E_z and H_z

$$E_x = -\frac{j}{\kappa^2} \left(\beta \frac{\partial E_z}{\partial x} + \omega \mu \frac{\partial H_z}{\partial y} \right) \quad (\text{A.29})$$

$$E_y = -\frac{j}{\kappa^2} \left(\beta \frac{\partial E_z}{\partial y} - \omega \mu \frac{\partial H_z}{\partial x} \right) \quad (\text{A.30})$$

$$H_x = -\frac{j}{\kappa^2} \left(\beta \frac{\partial H_z}{\partial x} - \omega \varepsilon \frac{\partial E_z}{\partial y} \right) \quad (\text{A.31})$$

$$H_y = -\frac{j}{\kappa^2} \left(\beta \frac{\partial H_z}{\partial y} + \omega \varepsilon \frac{\partial E_z}{\partial x} \right) \quad (\text{A.32})$$

where the propagation constant κ and wavenumber k are defined as

$$\kappa^2 = k^2 - \beta^2 \quad (\text{A.33})$$

$$k^2 = \omega^2 \varepsilon \mu \quad (\text{A.34})$$

Replacing H_x and H_y in (A.25) by (A.31) and (A.32) leads us to the Helmholtz's wave equations are given below

$$\frac{\partial^2 E_z}{\partial x^2} + \frac{\partial^2 E_z}{\partial y^2} + \kappa^2 E_z = 0 \Rightarrow \nabla^2 E_z + \kappa^2 E_z = 0 \quad (\text{A.35})$$

$$\frac{\partial^2 H_z}{\partial x^2} + \frac{\partial^2 H_z}{\partial y^2} + \kappa^2 H_z = 0 \Rightarrow \nabla^2 H_z + \kappa^2 H_z = 0 \quad (\text{A.36})$$

If the boundary conditions do not achieve coupling of these components, it is possible to obtain mode solutions with either $E_z = 0$ and $H_z = 0$. These modes are called respectively, Transverse Electric (TE) and Transverse Magnetic (TM) modes.

The propagation constant β has so far remained undetermined. Solution of the eigenvalues of the eigenvalue problem to find propagation constants is discussed in appendix-A4.

A.3 Guided Modes of the Slab Waveguide

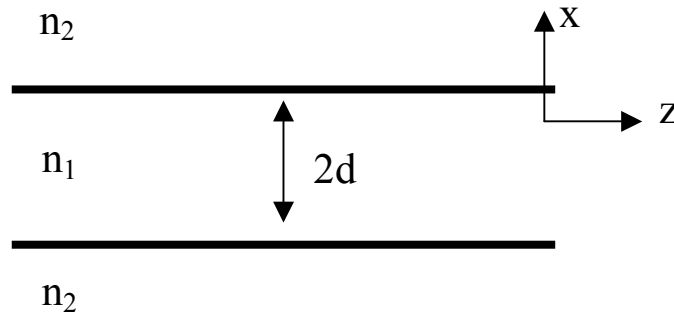


Figure A.1 Cross Sectional view of a Slab Waveguide.

Light transmission in a dielectric structure is an important part of the wave propagation in slab waveguides. Ridge refractive index is n_1 and cladding refractive index is given as n_2 . These are simpler dielectric waveguides, whose physical properties are nearly the same as round optical fiber, but those are much easier to analyze.

The radiation and mode conversion of slab waveguide are shown in figure A.1. We can simplify the discussion further by assuming that there is no variation of either waveguide geometry or the field distributions in y direction

$$\frac{\partial}{\partial y} = 0 \quad (\text{A.37})$$

This restriction allows us to decompose the field of the slab waveguide into TE and TM modes (TE and TM modes discussed earlier in chapter).

A.3.1 TE modes ($E_z = 0$; $H_z \neq 0$)

Here, with the derivation of the properties of TE modes are considered. Only H_z , H_x and E_y are nonzero field components according to equations (A.19) through (A.31). Using (A.37), (A.26), (A.27) and (A.28); these set of solutions are obtained

$$H_x = -\frac{j}{\omega\mu} \frac{\partial E_y}{\partial z} \quad (\text{A.38})$$

$$H_z = \frac{j}{\omega\mu} \frac{\partial E_y}{\partial x} \quad (\text{A.39})$$

E_y component is calculated as a solution of the wave equation

$$\frac{\partial^2 E_y}{\partial x^2} + \frac{\partial^2 E_y}{\partial z^2} + n^2 k_0^2 E_y = 0 \quad (\text{A.40})$$

with the refractive index

$$n^2 = \frac{\epsilon}{\epsilon_0} \quad (\text{A.41})$$

and

$$k_0 = \omega \sqrt{\epsilon_0 \mu_0} = \frac{2\pi}{\lambda_0} \quad (\text{A.42})$$

With the time and z dependence $e^{j(\omega t - \beta z)}$ we have

$$\frac{\partial^2 E_y}{\partial x^2} + (n^2 k_0^2 - \beta^2) E_y = 0 \quad (\text{A.43})$$

Because of different refractive index values, solution of this equation inside the slab is different from the solution in the cladding medium. If the modes from start into even and odd modes are separated, this treatment could be simplified.

A.3.1.1 Even Guided TE Modes

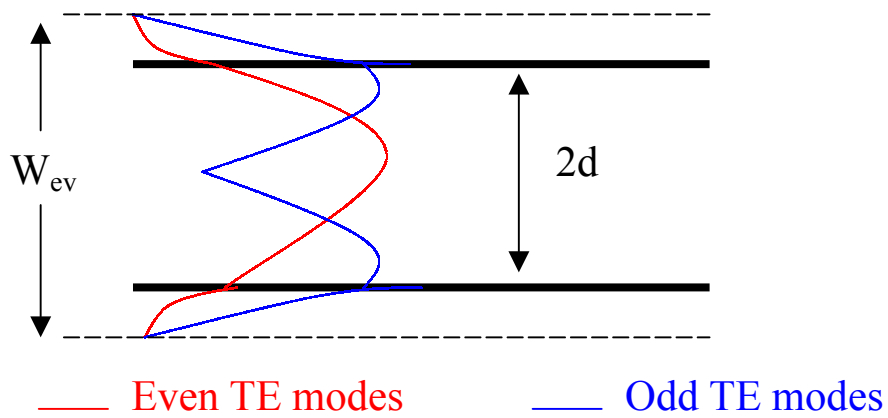


Figure A.2 Even TE and Odd TE modes of slab waveguide.

The mode solution for even modes inside the slab $|x| < d$ is given by

$$E_y = A_e \cos(\kappa x) \quad (\text{A.44})$$

$$H_z = -\frac{j\kappa}{\omega\mu_0} A_e \sin(\kappa x) \quad (\text{A.45})$$

with

$$\kappa^2 = n_1^2 k_0^2 - \beta^2 \quad (\text{A.46})$$

The field outside the slab (cladding region) $|x| > d$ is written as

$$E_y = A_e \cos(\kappa d) e^{-\gamma(|x|-d)} \quad (\text{A.47})$$

$$H_z = -\frac{x}{|x|} \frac{j\gamma}{\omega\mu_0} A_e \cos(\kappa d) e^{-\gamma(|x|-d)} \quad (\text{A.48})$$

with

$$\gamma^2 = \beta^2 - n_2^2 k_0^2 \quad (\text{A.49})$$

If $n_1 > n_2 \Rightarrow \kappa^2$ and β^2 are both positive quantities, thus these modes are propagating modes. E_y Component must be continuous at $x = \pm d$. Also H_z component crossing the interface between the two media must be continuous. These are boundary conditions. So we obtain from (A.9) and (A.12), the eigenvalue equation is

$$\tan(\kappa d) = \frac{\gamma}{\kappa} \quad (\text{A.50})$$

A.3.1.2 Odd Guided TE Modes

Odd modes are obtained very similar to even TE modes. The field inside the slab for $|x| < d$

$$E_y = A_o \sin(\kappa x) \quad (\text{A.51})$$

$$H_z = \frac{j\kappa}{\omega\mu_0} A_o \cos(\kappa x) \quad (\text{A.52})$$

The fields outside the slab $|x| > d$ are given by

$$E_y = \frac{x}{|x|} A_o \sin(\kappa d) e^{-\gamma(|x|-d)} \quad (\text{A.53})$$

$$H_z = -\frac{j\gamma}{\omega\mu_0} A_o \sin(\kappa d) e^{-\gamma(|x|-d)} \quad (\text{A.54})$$

If we use the boundary conditions, the eigenvalue equation for odd TE modes are obtained

$$\tan(\kappa d) = -\frac{\kappa}{\gamma} \quad (\text{A.55})$$

A.3.1.3 Eigenvalues of TE Modes

Solution of eigenvalue equations (A.50) and (A.55) cannot be found easily by using analytical expressions. A good method is graphical solution of equations. If both left-hand and right-hand of these equations are plotted, when at intersections of curves, solutions can be obtained. The function γ/κ is obtained from (A.46) and (A.49)

$$\frac{\gamma}{\kappa} = \frac{\sqrt{(n_1^2 - n_2^2)k_0^2 - \kappa^2}}{\kappa} \quad (\text{A.56})$$

The cutoff condition for the even TE modes is obtained from the requirement that the end point of γ/κ on the (κd) axis coincides with the zero crossing of the tangent function.

$$(\kappa_c d) = \nu\pi \quad (\text{A.57})$$

where ν is integer number.

We find the cutoff condition from (A.20)

$$\sqrt{n_1^2 - n_2^2} k_0 d = \nu\pi = \kappa_c d \quad (\text{A.58})$$

At cutoff, $\beta = n_2 k_0$.

$$\frac{\beta_c}{\kappa_c} = \frac{n_2}{\sqrt{n_1^2 - n_2^2}} \quad (\text{A.59})$$

A.3.2 TM Modes ($E_z \neq 0$; $H_z = 0$)

The only non vanishing field components can be found from equations (A.29), (A.30), (A.31), (A.32) and (A.37)

$$E_x = \frac{j}{n^2 \omega \epsilon_0} \frac{\partial H_y}{\partial z} \quad (\text{A.60})$$

$$E_z = -\frac{j}{n^2 \omega \epsilon_0} \frac{\partial H_y}{\partial x} \quad (\text{A.61})$$

H_y Component of field can be obtained from wave equation

$$\frac{\partial^2 H_y}{\partial x^2} + (n^2 k_0^2 - \beta^2) H_y = 0 \quad (\text{A.62})$$

A.3.2.1 Even Guided TM Modes

The even TM modes inside the slab $|x| < d$ are given by

$$H_y = B_e \cos(\kappa x) \quad (\text{A.63})$$

$$E_z = \frac{j\kappa}{n_1^2 \omega \epsilon_0} B_e \sin(\kappa x) \quad (\text{A.64})$$

The field components outside the slab $|x| > d$ are

$$H_y = B_e \cos(\kappa x) e^{-\gamma(|x|-d)} \quad (\text{A.65})$$

$$E_z = \frac{x}{|x|} \frac{j\gamma}{n_2^2 \omega \epsilon_0} B_e \cos(\kappa d) e^{-\gamma(|x|-d)} \quad (\text{A.66})$$

The eigenvalue equation is obtained from the requirement that E_z remain continuous at $x = \pm d \Rightarrow$

$$\tan(\kappa d) = \frac{n_1^2 \gamma}{n_2^2 \kappa} \quad (\text{A.67})$$

A.3.2.2 Odd Guided TM Modes

The field of the odd TM when $|x| < d$ is written as

$$H_y = B_o \sin(\kappa x) \quad (\text{A.68})$$

$$E_z = -\frac{j\kappa}{n_1^2 \omega \epsilon_0} B_o \cos(\kappa x) \quad (\text{A.69})$$

The field for outside of slab $|x| > d$ is given by

$$H_y = \frac{x}{|x|} B_o \sin(\kappa d) e^{-\gamma(|x|-d)} \quad (\text{A.70})$$

$$E_z = \frac{j\gamma}{n_2^2 \omega \epsilon_0} B_o \sin(\kappa d) e^{-\gamma(|x|-d)} \quad (\text{A.71})$$

If we use boundary conditions, the eigenvalue equation is found as

$$\tan(\kappa d) = -\frac{n_2^2 \kappa}{n_1^2 \gamma} \quad (\text{A.72})$$

A.4 Solution of Eigenvalue Equations

The properties of the guided modes are determined by the values of their propagation constants. In this section, an approximation method to find propagation constants of both TE modes is discussed. Firstly TE modes of the structure are considered. The even TE modes are obtained from the eigenvalue equation

$$\tan(\kappa d) = \frac{\gamma}{\kappa} \quad (\text{A.73})$$

The odd TE modes are obtained from the equation

$$\tan(\kappa d) = -\frac{\kappa}{\gamma} \quad (\text{A.74})$$

With using a constant C defined as

$$C = \sqrt{(n_1^2 - n_2^2) k_0 d} \quad (\text{A.75})$$

The relation between κ , d and V can be found by using equations (A.72), (A.73) and (A.74) as follows

$$(\kappa d)^2 + (\gamma d)^2 = C^2 \quad (\text{A.76})$$

At cutoff $\gamma d = 0$, from the equation (A.75) we have seen that the cutoff values of (κd) and C are identical

$$(\kappa d)_c = C_c = v \frac{\pi}{2} \quad v = 0, 1, 2, 3, \dots \quad (\text{A.77})$$

Expressing (κd) and (γd) in the form

$$\kappa d = v \frac{\pi}{2} + \eta \quad (\text{A.78})$$

$$\gamma d = v \frac{\pi}{2} \eta \quad (\text{A.79})$$

with $\eta \ll 1$ for even TE modes (v even).

From (A.75) and (A.77)

$$\eta = C - v \frac{\pi}{2} \quad (\text{A.80})$$

Near cutoff solution is

$$\gamma d = v \frac{\pi}{2} \left(C - v \frac{\pi}{2} \right) \quad (\text{A.81})$$

The near cutoff solution is valid for both even and odd TE modes of the slab waveguide. The only exception to this rule is the lowest order TE mode whose cutoff frequency is zero. Near cutoff, we have $\kappa d \ll 1$ for the lowest order even mode

$$\gamma d = (\kappa d)^2 \quad (\text{A.82})$$

If replacing the (κd) with equation (a.75)

$$\gamma d = \frac{1}{2} \left(\sqrt{4C^2 + 1} - 1 \right) \quad (\text{A.83})$$

The propagation constant is obtained in (A.48). With using (A.81) we obtain near cutoff expression for the even and odd TE modes with the exception of the lowest order mode, the approximation is

$$\beta d = \sqrt{(n_2 k_o d)^2 + v^2 \frac{\pi}{4} \left(C - v \frac{\pi}{2} \right)^2} \quad (\text{A.84})$$

For the even (lowest order) TE mode, we obtain from (A.49) and (A.83)

$$\beta d = \sqrt{(n_2 k_o d)^2 + \frac{1}{2} \left(1 + 2C^2 - \sqrt{1 - 4C^2} \right)} \quad (\text{A.85})$$

We consider (κd) as a function of C , and take the C derivative of (A.72)

$$\frac{1}{\cos^2(\kappa d)} \frac{\partial(\kappa d)}{\partial C} = -\frac{\gamma d}{(\kappa d)^2} \frac{\partial(\kappa d)}{\partial C} + \frac{C - (\kappa d)}{(\kappa d)(\gamma d)} \frac{\partial(\kappa d)}{\partial C} \quad (\text{A.86})$$

To express (γd) in terms of (κd) and C , (A.4) could be used. From (A.1) and (a.75)

$$\cos^2(\kappa d) = \frac{(\kappa d)^2}{C^2} = \frac{\kappa^2}{(n_1^2 - n_2^2) k_0} \quad (\text{A.87})$$

This allows us to express (2.86) in the form of

$$\frac{\partial(\kappa d)}{\partial C} = \frac{\kappa d}{C(1 + \gamma d)} \quad (\text{A.88})$$

Far from cutoff, we have $\gamma d \gg 1$ and $C \gg 1$, so that we obtain from (A.75) the approximation $\gamma d = C$. Equation (A.88) can be approximated

$$\frac{\partial(\kappa d)}{\partial C} = \frac{\kappa d}{C(1+C)} \quad (\text{A.89})$$

For $C \rightarrow \infty$ we have seen that for even and odd TE modes we have the eigenvalue equation for TE modes

$$\kappa = \frac{(\nu+1)\pi}{2d} \quad (\text{A.90})$$

This lateral wavenumber (A.90) is used to generate the MMI approach for optical slab waveguides.

A.5 Goos - Haenchen Shift

If you send a beam into two dielectric media, whose reflection coefficients are different (actually $n_1 > n_2$), when the beam passes through the one interface to other, the reflection of beam changes little different. There is a displacement of direction of reflected beam.

Because of a virtual surface, which is parallel to actual interface, it exists. This virtual surface causes displacement. It is not expected to be in accordance with the geometric theory.

In 1947, Goos and Haenchen made an experiment to formulate the displacement. This effect is known as the Goos-Haenchen shift. It is found that waveguide concepts contribute significantly to the basic theory of this interesting shift.

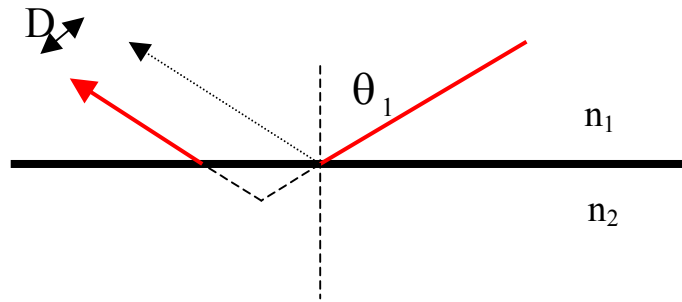


Figure A.3 The Goos-Hanchen shift D of a beam of reflected light.

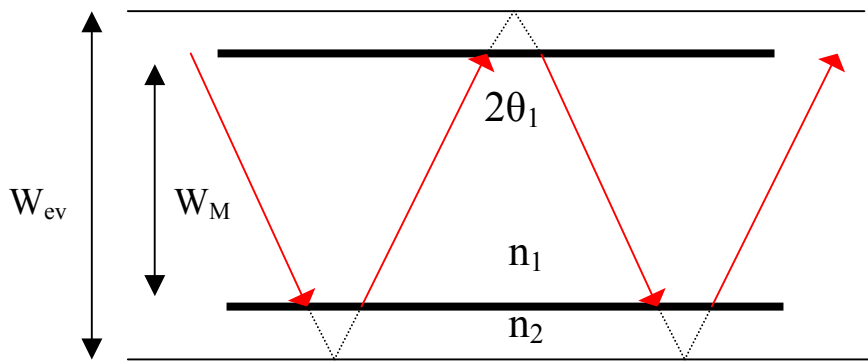


Figure A.4 Goos-Hanchen shifts on the waveguide.

W_{ev} "Effective Width" associated with Goos-Hanchen shift is given as

For TE modes:

$$W_{ev} - W_M = \frac{\lambda_0}{\pi (n_1^2 \sin^2 \theta_1 - n_2^2)^{1/2}} \quad (\text{A.91})$$

For TM modes:

$$W_{ev} - W_M = \frac{[\lambda_0 n_2^2 / n_1^2]}{\pi (n_1^2 \sin^2 \theta_1 - n_2^2)^{1/2}} \quad (\text{A.92})$$

W_M is physical width of the waveguide.

APPENDIX B

ANALYSIS OF RECTANGULAR WAVEGUIDES

The rectangular waveguide with a cross section as illustrated in figure A-1 is an example of a waveguiding device that will not support a TEM wave.

Consequently, it turns out that unique voltage and current waves do not exist, and the analysis of the waveguide properties has to be carried out as a field problem rather than as a distributed-parameter-circuit problem.

Collin has investigated the field analyses for both TE and TM waves and also derived propagation constants in a rectangular waveguide [18]. The essential properties of empty loss-free waveguides are that there is a double infinity of possible solutions for both TE and TM waves. The solutions are called *propagation modes*.

These waves or modes may be labeled by two identifying integer subscripts n and m , for example, TE_{nm} . These integers pertain to the number of standing-wave interference maxima occurring in the field solutions that describe the variation of the fields along the two transverse coordinates.

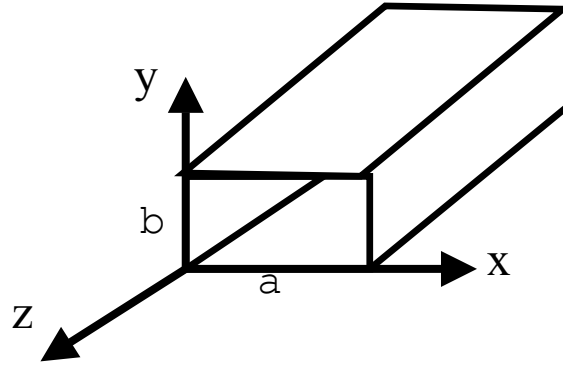


Figure B-1 Cross section of rectangular waveguide.

It is pointed that each mode has associated with a characteristic cutoff frequency $f_{c, nm}$ below which the mode does not propagate and above which the mode does propagate. The cutoff frequency is a geometrical parameter depending on the waveguide cross-sectional configuration. When f_c has been determined, it is found that the propagation factor is given by

$$\beta = (k_0^2 - k_c^2)^{1/2} \quad (\text{B.1})$$

where $k_0 = \omega \sqrt{\mu_0 \epsilon_0}$ and $k_c = 2\pi f_c \sqrt{\mu_0 \epsilon_0}$.

The guide wavelength is

$$\lambda_g = \frac{2\pi}{\beta} = \frac{\lambda_0}{\left(1 - \frac{\lambda_0^2}{\lambda_c^2}\right)^{1/2}} = \frac{\lambda_0}{\sqrt{1 - f_c^2/f^2}} \quad (\text{B.2})$$

where λ_0 is the free-space wavelength of plane waves at the frequency $f = \omega/2\pi$.

Since k_c differs for different modes, there is always a lower band of frequencies for which only one mode propagates.

If the guide is very long, considerable signal distortion may take place. The case of TE modes in a loss-free empty rectangular guide is considered first.

B.1. TE Waves

For *TE* or *H* modes, $e_z = 0$ and all the remaining field components can be determined from the axial magnetic field h_z . The axial field h_z is a solution of Helmholtz's equation

$$\nabla_t^2 h_z + k_c^2 h_z = 0 \quad (\text{B.3})$$

or

$$\frac{\partial^2 h_z}{\partial x^2} + \frac{\partial^2 h_z}{\partial y^2} + k_c^2 h_z = 0 \quad (\text{B.4})$$

If a product solution $h_z = f(x)g(y)$ is assumed, (B-4) becomes

$$\frac{1}{f} \frac{d^2 f}{dx^2} + \frac{1}{g} \frac{d^2 g}{dy^2} + k_c^2 = 0 \quad (\text{B.5})$$

After substituting fg for h_z and dividing the equation by fg .

The term $\frac{1}{f} \frac{d^2 f}{dx^2}$ is a function of x only, $\frac{1}{g} \frac{d^2 g}{dy^2}$ is a function of y only, and k_c^2 is a constant and hence this equation can hold for all values of x and y only if each term is constant.

Thus we may write

$$\frac{1}{f} \frac{d^2 f}{dx^2} = -k_x^2 \quad \text{or} \quad \frac{1}{f} \frac{d^2 f}{dx^2} + k_x^2 f = 0 \quad (\text{B.6})$$

$$\frac{1}{g} \frac{d^2 g}{dy^2} = -k_y^2 \quad \text{or} \quad \frac{1}{g} \frac{d^2 g}{dy^2} + k_y^2 g = 0 \quad (\text{B.7})$$

where $k_x^2 + k_y^2 = k_c^2$ in order that the sum of the three terms may vanish. The use of the separation of variables technique has reduced the partial differential equation (B-4) to the ordinary simple-harmonic second order equations. The solution of f and g are easily seen to be

$$f = A_1 \cos(k_x x) + A_2 \sin(k_x x) \quad (\text{B.8})$$

$$g = B_1 \cos(k_y y) + B_2 \sin(k_y y) \quad (\text{B.9})$$

where A_1 , A_2 , B_1 and B_2 are arbitrary constants. Since the normal component of the transverse magnetic field \mathbf{h} must vanish at the perfectly conducting waveguide wall and when this condition is true, tangential \mathbf{e} will also vanish on the guide walls.

The requirement, boundary conditions on h_z are given by

$$\frac{\partial h_z}{\partial x} = 0 \quad \text{at } x = 0, a \quad (\text{B.10})$$

$$\frac{\partial h_z}{\partial y} = 0 \quad \text{at } y = 0, b \quad (\text{B.11})$$

In the solution of f function, the boundary conditions give us

$$-k_x A_1 \sin(k_x x) + k_x A_2 \cos(k_x x) = 0 \quad \text{at } x = 0, a$$

Hence, from the condition that $x=0$, it is found that $A_2=0$. At $x=a$, it is necessary for $\sin(k_x a)=0$, and this says k_x to have the values

$$k_x = \frac{n\pi}{a} \quad n = 0, 1, 2, \dots \quad (\text{B.12})$$

In a similar solution it is found that $B_2=0$ and

$$k_y = \frac{m\pi}{b} \quad m = 0, 1, 2, \dots \quad (\text{B.13})$$

It is noted that when both n and m are zero, it yields a constant solution for h_z and no other field components exists. So this solution is of no interest.

If we use the above relations and put $A_1 B_1 = A_{nm}$, the solutions for h_z are seen to be

$$h_z = A_{nm} \cos\left(\frac{n\pi x}{a}\right) \cos\left(\frac{m\pi y}{b}\right) \quad (\text{B.14})$$

For the nm th mode, the cutoff wave number is given by

$$k_{c,nm} = \left[\left(\frac{n\pi}{a}\right)^2 + \left(\frac{m\pi}{b}\right)^2 \right]^{1/2} \quad (\text{B.15})$$

It is clearly a function of the guide dimensions only. The propagation constant for the nm mode is given by

$$\begin{aligned} \gamma_{nm} &= j\beta_{nm} = j(k_0^2 - k_{c,nm}^2)^{1/2} \\ &= j \left[\left(\frac{2\pi}{\lambda_0}\right)^2 - \left(\frac{n\pi}{a}\right)^2 - \left(\frac{m\pi}{b}\right)^2 \right]^{1/2} \end{aligned} \quad (\text{B.16})$$

When $k_0 > k_{c, nm}$, β_{nm} is pure real and the mode propagates; when $k_0 < k_{c, nm}$, then γ_{nm} is real but β_{nm} is imaginary and the propagation factor is $e^{-\gamma_{nm}|z|}$, which shows that the mode decays rapidly with distance $|z|$ from the point at which it is excited.

The frequency separating the propagation and decaying bands are designated as the cutoff frequency $f_{c, nm}$.

This is given by the equation

$$f_{c, nm} = \frac{c}{\lambda_{c, nm}} = \frac{c}{2\pi} k_{c, nm} = \frac{c}{2\pi} \left[\left(\frac{m\pi}{a} \right)^2 + \left(\frac{m\pi}{b} \right)^2 \right]^{1/2} \quad (\text{B.17})$$

where c is the velocity of light. The cutoff wavelength is defined as

$$\lambda_{c, nm} = \frac{2ab}{(n^2b^2 + m^2a^2)^{1/2}} \quad (\text{B.18})$$

B.2 TM Waves

For the TM Modes, h_z equals zero and e_z plays the role of a potential function from which the remaining field components may be derived. This axial electric field satisfies the reduced Helmholtz's equation

$$\nabla_t^2 e_z + k_c^2 e_z = 0 \quad (\text{B.19})$$

of the same type defined earlier for h_z , that is (B-4). The solution may be found by using the separation of variables method. In the present case

the boundary conditions require that e_z vanish at $x=0,a$ and $y=0,b$. This condition requires that the solution for e_z be

$$e_z = A_{nm} \sin\left(\frac{n\pi x}{a}\right) \sin\left(\frac{m\pi y}{b}\right) \quad (\text{B.20})$$

Instead of a product of cosine functions which was suitable for describing h_z . Again there are a doubly infinite number of solutions corresponding to various integers n and m .

However unlike the situation for TE modes, $n=0$ and $m=0$ are not solutions for the rectangular waveguides. The cutoff wave number is given by the same expression as for the TE modes; that is

$$k_{c, nm} = \left[\left(\frac{n\pi}{a}\right)^2 + \left(\frac{m\pi}{b}\right)^2 \right]^{1/2} \quad (\text{B.21})$$

and the propagation constant β_{nm} is given by the formula

$$\beta_{nm} = (k_0^2 - k_{c, nm}^2)^{1/2} \quad (\text{B.22})$$

APPENDIX C

ANALYSIS OF DIELECTRIC IMAGE LINES

A theoretical model for the rectangular dielectric waveguides is presented in this section.

Dielectric rectangular guides for optical frequencies have been described theoretically by Marcatili [21]. The propagation characteristics of the dielectric image guide and directional coupler have determined by Knox and Toullos [7].

Cross section of dielectric image lines is depicted in figure C.1. A rigorous solution to the boundary-value problem of a rectangular image guide using Maxwell's equations is extremely complex. However, it is possible to simplify this problem by solving two dielectric slab guides. For well-guided modes, the field decays exponentially outside the waveguide and most of the power travels inner side of the waveguide as given in figure C.2.

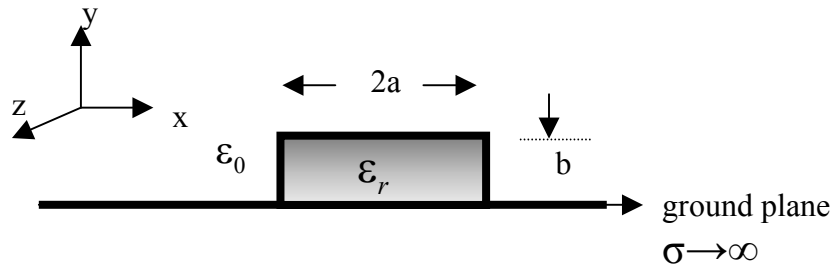


Figure C.1 Dielectric image guide.

Figure C.1 illustrates a dielectric image guide, which consists of a rectangular core of relative dielectric constant ϵ_r , surrounded by a semi-infinite medium of dielectric constant ϵ_0 and standing on a perfectly conducting ground plane. The direction of propagation is in the z direction. The main transverse field components of the E_{mn}^y modes are E_y and H_z . They are given in figure C.3 for the fundamental mode E_{11}^y . Within the guiding rod each component varies sinusoidally both along x and along y directions. Outside the guide each component decays exponentially as shown in the figure C.3.

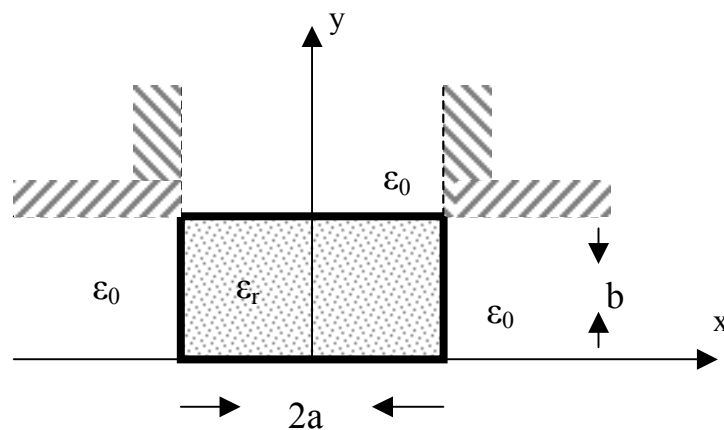


Figure C.2 Cross section of image guide.

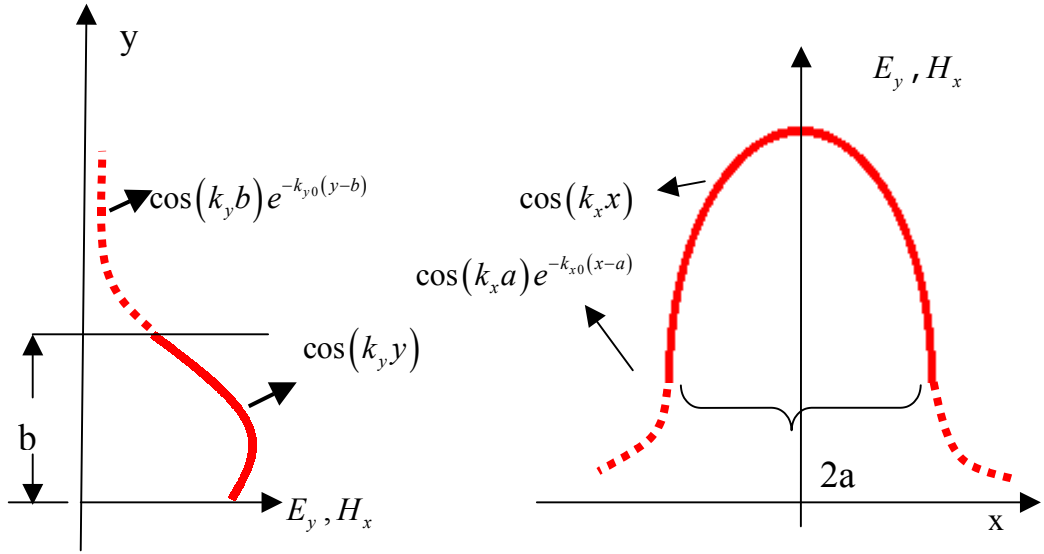


Figure C.3 Field Distribution of the fundamental mode E_{11}^y .

The transverse propagation constant k_x and k_y are solutions of the transcendental equations

$$ak_x = \frac{m\pi}{2} - \tan^{-1}\left(\frac{k_x}{k_{x0}}\right), \quad m = 1, 2, 3, \dots \quad (\text{C.1})$$

$$bk_y = \frac{n\pi}{2} - \tan^{-1}\left(\frac{k_y}{\epsilon_r k_{y0}}\right), \quad n = 1, 2, 3, \dots \quad (\text{C.2})$$

$$k_{x0} = [(\epsilon_{re} - 1)k_0^2 - k_x^2]^{1/2} \quad (\text{C.3})$$

$$k_{y0} = [(\epsilon_r - 1)k_0^2 - k_y^2]^{1/2} \quad (\text{C.4})$$

$$\epsilon_{re} = \epsilon_r - (k_y/k_0)^2 \quad (\text{C.5})$$

$$k_0 = \frac{2\pi}{\lambda_0} \quad (\text{C.6})$$

λ_0 is the free-space wavelength.

Having determined k_x and k_y from equations C.1 and C.2, the axial propagation constant k_z is given as

$$k_z = \left(k_0^2 \epsilon_{re} - k_x^2 \right)^{1/2}$$

APPENDIX D

MATLAB CODES

```
%-----  
%-----  
% Simulation of MMI Optical Devices.  
% This program uses the propagation constant formulation of optical slab  
% waveguides (A.90) and MMI formulation (2.18).  
%-----  
%-----  
clear all;  
clc;  
a = 16; %We  
nr = 1.673; %indexes  
nc = 1.444;  
f = 20*(10^9); %Operational frequency  
x3=linspace(0,a,500);  
% generating original signal  
n=1:101 ;  
x=sin((n-1)*pi/100) ;  
x1=ones(101,1);  
dim=length(x) ;  
y1=zeros(1,dim*5) ;  
y1(1,dim*1:dim*2-1)=x ;  
y2=zeros(1,dim*5) ;  
y2(dim*2:dim*3-1)=x1;  
y2(dim*4:dim*5-1)=x1;  
  
y=y1;  
y1=y(1:500);  
secim = 1;  
  
N = 500;  
W0 = (2*pi)/500;  
  
% finding fourier series coefficients  
for k =1:500  
    sum = 0;  
    for n =1:500
```

```

    u(k) = y(n)*exp(-i*(k-1)*W0*(n-1));
    sum = u(k) + sum ;
end
x_u(k) = sum;
end
x_u=fftshift(x_u);
x=x_u(250:400);

c = 3*(10^10);
dalgaboyu = c/f; %centimetre
k0 = (2*pi)/dalgaboyu;
NA = sqrt((nr^2)-(nc^2)); %lateral numerical aperture
u = (dalgaboyu/pi)*((nc/nr)^(2*secim))*(1/NA);
Wev = a+u; %effective width
Lpi = (4*nr*(Wev^2))/(3*dalgaboyu); %beat length
L = Lpi*1.5;
beta2 = k0*nr-((9*pi*dalgaboyu)/(4*nr*Wev*Wev));
beta0 = k0*nr-((1*pi*dalgaboyu)/(4*nr*Wev*Wev));
beta1 = k0*nr-((4*pi*dalgaboyu)/(4*nr*Wev*Wev));
Lt = pi/(beta0-beta2);
%-----
%Finding number of modes and resolution
V = ((2*pi)/dalgaboyu)*a*sqrt((nr^2)-(nc^2));
m = V/pi;
m = round(m);
resolution = Wev/m;
%-----
% MMI Part
for n = 1:500
    sum = 0;
    for k = 1:m
        b = x(k)*exp(i*(k-1)*(n-1)*W0)*exp(i*L*((k*(k+2)*pi)/(3*Lpi)));
        sum = sum + b;
    end
    c(n) = (sum/N)*(10/7.5);
end
plot(x3,y1);hold on;plot(x3,abs(c),'r*'); %plotting
hold;legend('input','output');
grid on;xlabel('x-axis');ylabel('y-label');

```

```

%-----
%-----
% Simulation of Normal Rectangular Waveguide systems with the MMI Method.
%This program uses propagation constants formulation of rectangular
%waveguides (3.10), (3.11) cutoff frequency formulation (B.17) and MMI
%formulation (3.9).
%-----
%-----

clear all;
clc;

%-----INPUTS-----
a = 6; % We
b = 1.016; % thickness.....
f0 = 27; % GHz Operational Frequency...
f0 = f0*(10^9);
c = 3*(10^10); %Speed...
lambda = c/f0 %Wavelength....

x2=linspace(0,a,500); % x-axis...
y2=linspace(0,b,500); % y-axis....
y=exp(-5)*(x2-(a/2)).^2); % Waveform

%----FINDING PROPAGATION CONSTANTS----
m2 = 10;
n2 = 0;

for m = 1:m2

    kx(m)= ((m*pi)/a);
    ky(m) = ((n2*pi)/b);
    kt = (2*pi/lambda);
    kz(m) = sqrt( kt*kt - kx(m)^2 - ky(m)^2);

    fc(m) = (c/2*pi)*sqrt(kx(m)^2 + ky(m)^2); % cutoff - frequencies
end

kz1=kz;

%-----Generating Modes-----

Ey = zeros(10,500);

```

```

for m=1:10
    Ey(m,1:500)=sin(kx(m).*x2).*cos(ky(m).*y2);
    %Ey = sin(kx.x).cos(ky.y) olarak hesaplandı
end

%-----Field Excitation Coefficients (Cv)----

c1=sum(y.*Ey(1,1:500))./sqrt(sum(Ey(1,1:500).*Ey(1,1:500)));
c2=sum(y.*Ey(2,1:500))./sqrt(sum(Ey(2,1:500).*Ey(2,1:500)));
c3=sum(y.*Ey(3,1:500))./sqrt(sum(Ey(3,1:500).*Ey(3,1:500)));
c4=sum(y.*Ey(4,1:500))./sqrt(sum(Ey(4,1:500).*Ey(4,1:500)));
c5=sum(y.*Ey(5,1:500))./sqrt(sum(Ey(5,1:500).*Ey(5,1:500)));

d1=sum(y.*Ey(6,1:500))./sqrt(sum(Ey(6,1:500).*Ey(6,1:500)));
d2=sum(y.*Ey(7,1:500))./sqrt(sum(Ey(7,1:500).*Ey(7,1:500)));
d3=sum(y.*Ey(8,1:500))./sqrt(sum(Ey(8,1:500).*Ey(8,1:500)));
d4=sum(y.*Ey(9,1:500))./sqrt(sum(Ey(9,1:500).*Ey(9,1:500)));
d5=sum(y.*Ey(10,1:500))./sqrt(sum(Ey(10,1:500).*Ey(10,1:500)));

y11 = c1*Ey(1,1:500)+c2*Ey(2,1:500)+c3*Ey(3,1:500)...
    +c4*Ey(4,1:500)+c5*Ey(5,1:500)+d1*Ey(6,1:500)+d2*Ey(7,1:500)...
    +d3*Ey(8,1:500)+d4*Ey(9,1:500)+d5*Ey(10,1:500);
max2=max(y11);
y11 = y11./max2;
Lpi = pi/(kz1(1)-kz1(2)) % Lpi.....
L = Lpi*(0);

% .....MMI Method .....
for n=0:9
    a11=exp(-j*kz1(1)*L)*(Ey(1,1:500).*exp(j*(kz1(1)-kz1(1))*L));
    a22=exp(-j*kz1(1)*L)*(Ey(2,1:500).*exp(j*(kz1(1)-kz1(2))*L));
    a33=exp(-j*kz1(1)*L)*(Ey(3,1:500).*exp(j*(kz1(1)-kz1(3))*L));
    a44=exp(-j*kz1(1)*L)*(Ey(4,1:500).*exp(j*(kz1(1)-kz1(4))*L));
    a55=exp(-j*kz1(1)*L)*(Ey(5,1:500).*exp(j*(kz1(1)-kz1(5))*L));

    b11=exp(-j*kz1(1)*L)*(Ey(6,1:500).*exp(j*(kz1(1)-kz1(6))*L));
    b22=exp(-j*kz1(1)*L)*(Ey(7,1:500).*exp(j*(kz1(1)-kz1(7))*L));
    b33=exp(-j*kz1(1)*L)*(Ey(8,1:500).*exp(j*(kz1(1)-kz1(8))*L));
    b44=exp(-j*kz1(1)*L)*(Ey(9,1:500).*exp(j*(kz1(1)-kz1(9))*L));
    b55=exp(-j*kz1(1)*L)*(Ey(10,1:500).*exp(j*(kz1(1)-kz1(10))*L));

rc=c1*a11+c2*a22+c3*a33+c4*a44+c5*a55+d1*b11+...
    d2*b22+d3*b33+d4*b44+d5*b55;
c00=abs(max(y)-max(rc));

```

```

c0=sum(y)/max(size(x2));% normalization
rcc=rc+c0;
arc=abs(rcc);
max2 = max(arc);
arc = arc./max2;

figure(1); % Plotting
subplot(10,1,(n+1));plot(x2,y);hold on; plot(x2,arc,'r');hold;
n=n+1;
d=Lpi*.1;
L=L+d
end

figure(2);
subplot(5,1,1);plot(x2,Ey(1,1:500),x2,Ey(2,1:500));
legend('Ey10','Ey20');
subplot(5,1,2);plot(x2,Ey(3,1:500),x2,Ey(4,1:500));
legend('Ey30','Ey40');
subplot(5,1,3);plot(x2,Ey(5,1:500),x2,Ey(6,1:500));
legend('Ey50','Ey60');
subplot(5,1,4);plot(x2,Ey(7,1:500),x2,Ey(8,1:500));
legend('Ey70','Ey80');
subplot(5,1,5);plot(x2,Ey(9,1:500),x2,Ey(10,1:500));
legend('Ey90','Ey100');

```

```

%-----
%-----
% Simulation of Dielectric Rectangular Waveguide Systems with the MMI
%Method.
% This program uses the propagation constants formulation of dielectric image
%guides (4.1), (4.2), (4.3) and MMI formulation (3.9).
%-----
%-----

```

```

clear all;
clc;

```

```

%-----INPUTS-----
a = 5; % We
ebe = .3; %thickness.....
Er = 2.28; % dielectric Constant....
f0 = 35; % GHz Operational frequency
f0 = f0*(10^9);
c = 3*(10^10);
lambda = c/f0 %Wavelength....

```

```

x2=linspace(0,a,500); % x-axis...
y2=linspace(0,ebe,500); % y-axis....
y=exp(-(5)*(x2-(a/2)).^2); % Waveform...

```

```

%----FINDING PROPAGATION CONSTANTS-----
m2 = 10;
n2 = 1;

```

```

% Finding propagation constants for each Em1 modes

```

```

    xk = -100:0.01:100;
    [f g] = size(xk);
    k0 = (2*pi)/lambda;

```

```

for m = 1:m2

```

```

    ky1 = n2*(pi/2)-atan(xk./(Er*sqrt((Er-1)*(k0*k0)-xk.*xk)));
    ky2 = ebe.*xk;
    ky3 = abs(ky1-ky2);
    [aa,bb] = min(ky3);
    ky(m) = xk(bb); % ky.....
    Ere = Er-((ky(m)/k0)^2);

```

```

    kx1 = m*(pi/2)-atan(xk./sqrt((Ere-1)*(k0*k0)-xk.*xk));

```

```

    kx2 = (a/2).*xk;
    kx3 = abs(kx1-kx2);
    [aaa,bbb] = min(kx3);
    kx(m) = xk(bbb); % kx.....

    kz(m)= sqrt(k0*k0*Ere-kx(m)*kx(m)-ky(m)*ky(m)); % kz
end

kz1=kz;

%-----Generating Modes.....

Ey = zeros(10,500);
for m=1:10
    Ey(m,1:500)=sin(kx(m). *x2).*cos(ky(m). *y2);
end

%-----Field Excitation Coefficients (Cv)

c1=sum(y.*Ey(1,1:500))./sqrt(sum(Ey(1,1:500).*Ey(1,1:500)));
c2=sum(y.*Ey(2,1:500))./sqrt(sum(Ey(2,1:500).*Ey(2,1:500)));
c3=sum(y.*Ey(3,1:500))./sqrt(sum(Ey(3,1:500).*Ey(3,1:500)));
c4=sum(y.*Ey(4,1:500))./sqrt(sum(Ey(4,1:500).*Ey(4,1:500)));
c5=sum(y.*Ey(5,1:500))./sqrt(sum(Ey(5,1:500).*Ey(5,1:500)));

d1=sum(y.*Ey(6,1:500))./sqrt(sum(Ey(6,1:500).*Ey(6,1:500)));
d2=sum(y.*Ey(7,1:500))./sqrt(sum(Ey(7,1:500).*Ey(7,1:500)));
d3=sum(y.*Ey(8,1:500))./sqrt(sum(Ey(8,1:500).*Ey(8,1:500)));
d4=sum(y.*Ey(9,1:500))./sqrt(sum(Ey(9,1:500).*Ey(9,1:500)));
d5=sum(y.*Ey(10,1:500))./sqrt(sum(Ey(10,1:500).*Ey(10,1:500)));

y11=c1*Ey(1,1:500)+c2*Ey(2,1:500)+c3*Ey(3,1:500)+c4*Ey(4,1:500)+c5*Ey(5,1:5
00)+d1*Ey(6,1:500)+d2*Ey(7,1:500)+d3*Ey(8,1:500)+d4*Ey(9,1:500)+d5*Ey(10,1
:500);
max2=max(y11);
y11 = y11./max2;
Lpi = pi/(kz1(1)-kz1(2)) % Lpi ....
L = Lpi*(0);

% .....MMI Method
for n=0:9
    a11=exp(-j*kz1(1)*L)*(Ey(1,1:500).*exp(j*(kz1(1)-kz1(1))*L));
    a22=exp(-j*kz1(1)*L)*(Ey(2,1:500).*exp(j*(kz1(1)-kz1(2))*L));

```

```

a33=exp(-j*kz1(1)*L)*(Ey(3,1:500).*exp(j*(kz1(1)-kz1(3))*L));
a44=exp(-j*kz1(1)*L)*(Ey(4,1:500).*exp(j*(kz1(1)-kz1(4))*L));
a55=exp(-j*kz1(1)*L)*(Ey(5,1:500).*exp(j*(kz1(1)-kz1(5))*L));

b11=exp(-j*kz1(1)*L)*(Ey(6,1:500).*exp(j*(kz1(1)-kz1(6))*L));
b22=exp(-j*kz1(1)*L)*(Ey(7,1:500).*exp(j*(kz1(1)-kz1(7))*L));
b33=exp(-j*kz1(1)*L)*(Ey(8,1:500).*exp(j*(kz1(1)-kz1(8))*L));
b44=exp(-j*kz1(1)*L)*(Ey(9,1:500).*exp(j*(kz1(1)-kz1(9))*L));
b55=exp(-j*kz1(1)*L)*(Ey(10,1:500).*exp(j*(kz1(1)-kz1(10))*L));

rc=c1*a11+c2*a22+c3*a33+c4*a44+c5*a55+d1*b11+d2*b22+d3*b33+d4*b44+
d5*b55;
c00=abs(max(y)-max(rc));
c0=sum(y)/max(size(x2));% normalization
rcc=rc+c0;
arc=abs(rcc);
max2 = max(arc);
arc = arc./max2;

figure(1); % Plotting
subplot(10,1,(n+1));plot(x2,y);hold on; plot(x2,arc,'r');hold;
n=n+1;
d=L*pi*.3;
L=L+d;
end

figure(2);
subplot(5,1,1);plot(x2,Ey(1,1:500),x2,Ey(2,1:500));
legend('Ey11','Ey21');
subplot(5,1,2);plot(x2,Ey(3,1:500),x2,Ey(4,1:500));
legend('Ey31','Ey41');
subplot(5,1,3);plot(x2,Ey(5,1:500),x2,Ey(6,1:500));
legend('Ey51','Ey61');
subplot(5,1,4);plot(x2,Ey(7,1:500),x2,Ey(8,1:500));
legend('Ey71','Ey81');
subplot(5,1,5);plot(x2,Ey(9,1:500),x2,Ey(10,1:500));
legend('Ey91','Ey101');

```